Tropical Cyclogenesis Sensitivity to Environmental Parameters in Radiative-Convective Equilibrium

David S. Nolan* and Eric D. Rappin

Rosenstiel School of Marine and Atmospheric Science

University of Miami

Miami, FL

and

Kerry A. Emanuel

Program in Atmospheres, Oceans, and Climate

Massachusetts Institute of Technology

Cambridge, MA

Submitted to *The Quarterly Journal of the Royal Meteorological Society*

January 8th, 2007

Revised, August 31st, 2007

*Corresponding author address: Prof. David S. Nolan, RSMAS/MPO, 4600 Rickenbacker Causeway, Miami, FL, 33149. email: dnolan@rsmas.miami.edu

Summary

In this study the relationship between the likelihood of tropical cyclogenesis and external environmental forcings is explored in the simplest idealized modeling framework possible: radiative-convective equilibrium on a doubly-periodic *f*-plane. In such an environment, control of the equilibrium enviromental sounding is reduced to three parameters: the sea-surface temperature, the Coriolis parameter, and the imposed background surface wind speed. Cloud-resolving mesoscale model simulations are used to generate environments of radiative-convective equilibrium determined by these three factors. The favorability of these environments for tropical cyclogenesis is measured in three ways: in terms of the maximum potential intensity (MPI) of the sounding, based on the thermodynamic theory of Emanuel; in terms of the "genesis potential" determined by an empirical genesis parameter; and in terms of the propensity of weak initial vortices in these environments to form into tropical cyclones.

The simulated environments of radiative-convective equilibrium with no vertical wind shear are found to be very favorable for tropical cyclogenesis. Weak initial vortices always transition to a tropical cyclone, even for rather low sea surface temperatures. However, the time required for these vortices to make the transition from a weak, mid-level vortex to a rapidly developing tropical cyclone decreases as the MPI increases, indicating the importance of MPI in enhancing the frequency of cyclogenesis. The relationship between this "time to genesis" and the thermodynamic parameters is explored. The time to genesis is found to be very highly (negatively) correlated to MPI, with little or no relationship to convective instability, Coriolis parameter, mid-level humidity, or the empirical genesis parameter.

In some cases, tropical cyclones are found to form spontaneously from random convection. This formation is due to a cooperative interaction between large-scale moisture, longwave radiation, and locally enhanced sea-surface fluxes, similar to the “aggregation” of convection found in previous studies.

Keywords: tropical cyclogenesis, convection, climate

1. Introduction

a. Background

In his textbook on general meteorology, Byers (1944) stated that "The processes bringing about the formation of tropical cyclones are not definitely known, although several plausible theories have been presented." In spite of the advent of greatly advanced observing capabilities, and the success of both highly simplified and highly sophisticated numerical models in reproducing (or seeming to reproduce) the formation and evolution of such storms, the internal processes of tropical cyclone (TC) genesis are still quite mysterious. Thus, to some extent, Byers' assessment of the problem remains valid after more than sixty years.

One approach to the problem is to study the development of individual cyclones using detailed mesoscale observations with the goal of understanding the sequence of events leading to a developing storm, such as in the studies of Bister and Emanuel (1997), Simpson et al. (1997), Reasor et al. (2005), and Sippel et al. (2006). Much of what cannot be seen by instruments can be illustrated in highly resolved numerical simulations of genesis, as in Davis and Bosart (2001, 2002) and Hendricks et al. (2004). Although there is a notable lack of documentation of non-developing systems, much has been learned from these studies.

As another way to understand TC genesis, one may approach the problem from the "other end" by investigating the relationship between the likelihood (or frequency) of genesis and large-scale enviromental factors. This area of research was arguably pioneered by Palmén (1948), who pointed out that tropical cyclones develop almost exclusively in regions where the sea surface temperature (SST) exceeds 26 ^{o}C, but was greatly advanced by Gray (1968, 1975), who included several other large-scale environmental predictors, such as wind shear and low-level vorticity (see

also DeMaria 2001). Along with the intended applications of understanding and predicting seasonal and regional trends in TC frequency, it is hoped that this approach will also lead to an understanding of how overall levels of tropical cyclone activity are controlled by climate, and to predictions about how such activity might change as climate evolves. A number of studies have assessed potential changes in future TC frequency by computing Gray's parameter for simulated atmospheres under various global warming scenarios (Ryan et. al. 1992; Royer et al. 1998; Sugi et al. 2002; McDonald et al. 2005). Due to its large sensitivity to SST relative to 26.5°C, Gray's parameter predicts a large and universal increase in TC activity with greenhouse warming. For this reason, Royer et al. (1998) developed a "convective" genesis parameter which replaced the thermodynamic part of Gray's parameter with a factor proportional to the model-simulated rainfall rate, as a proxy for convective activity. In subsequent studies, this modified parameter predicted changes in TC activity that were either small or negative, and that were more consistent with predictions of *decreased* TC counts under greenhouse warming in the same (higher resolution) simulations (McDonald et. al. 2005; Chauvin et al. 2006).

A second approach to understanding the distribution and frequency of TC genesis is simply that of counting the number of TCs simulated by global climate models in the present (to validate the model and to establish a baseline frequency) and in the future (according to various global warming scenarios). While the very low resolutions of the models used in the earliest attempts of TC counting (Bengtsson et al. 1982; Broccoli and Manabe 1990; Haarsma et al. 1993; Bengtsson et al. 1996) left considerable doubt as to their relevance (Evans 1992; Lighthill et al. 1994), the steady rise in computing power has more recently allowed global climate models to simulate TCs with some degree of realism (Sugi et al. 2002; McDonald et al. 2005; Chauvin et al. 2006; Yoshimura et al. 2006; Bengtsson et al. 2007). A consistent pattern that has emerged from

tropical cyclone counting in the most recent studies is one of decreasing global numbers of cyclones. Some of the studies also report that the intensity of the strongest storms will increase (Oouchi et al. 2006; Bengtsson et al. 2007) in agreement with theory (Emanuel 1987) and with earlier studies using regional models with environments predicted by GCMs (Knutson et al. 2001; Knutson and Tuleya 2004).

In this study, we step away from real-world conditions and seek to understand some of the large-scale influences on TC genesis in highly idealized, controlled environments in which the relevant large-scale variables can be varied individually. Specifically, we use a cloud-resolving numerical model to perform highly idealized simulations of convection and tropical cyclogenesis in environments of radiative-convective equilibrium (RCE). By RCE, we refer to an atmospheric equilibrium that results when the loss of energy to space by longwave radiation is balanced by the transfer of latent and sensible energy from the surface to the boundary layer, and its redistribution throughout the atmosphere by deep moist convection. While RCE shares certain characteristics of the tropics, such as very weak temperature gradients, warm temperatures, and sufficient moisture to support deep convection, it undoubtedly departs signicantly from the real tropical atmosphere: due to large-scale circulations like the Hadley cell and the Walker circulation, very little, if any, of the Earth's tropics are ever in a state of RCE.

Despite this caveat, we believe that RCE is a very useful point of reference from which to explore the effects of varying environments on TC genesis. Our view is perhaps best stated by Bretherton et al. (2005): "Radiative-convective equilibrium above a horizontally homogenous surface, with no ambient rotation or pressure gradients, is a time-honored idealization for understanding the tropical atmosphere and its sensitivity to perturbations in radiative or surface forcing, starting with single column models (Manabe and Strickler 1964) and moving on to three-dimen-

sional (3D) cloud resolving models (CRMs; e.g., Tompkins and Craig 1998).” On a more practical level, by using simulated environments of RCE, we can generate atmospheric states that depend on a minimal number of explicitly controlled parameters, rather than attempting to explore (or even define) the infinite space of all possible atmospheric temperature and humidity profiles over various SSTs.

The goal of this idealized modeling approach is to *isolate* the way in which the likelihood of tropical cyclogenesis varies with such parameters as environmental vorticity, mean surface wind, and the locally computed maximum potential intensity (MPI), which subsumes local variations of both SST and the overlying atmospheric temperature and moisture profile.

b. Working hypothesis

Our working hypothesis and simulation designs are motivated by recent progress in the empirical prediction of TC genesis and frequency. While the Gray index used an SST of 26.5°C as the marginal temperature above which TC genesis becomes increasingly likely, the development of various MPI theories has suggested that the “thermodynamic component” of the likelihood of tropical cyclogenesis is not a function of SST alone, but is also strongly dependent on the sounding of the the overlying atmosphere. Emanuel and Nolan (2004) presented a new genesis index which depends on MPI rather than SST itself, i.e.

$$GP = \left|10^5 \eta\right|^{\frac{3}{2}} \left(\frac{H}{50}\right)^3 \left(\frac{V_{\text{pot}}}{70}\right)^3 (1 + 0.1\, V_{shear})^{-2} \tag{1.1}$$

where the parameters are local mean values of absolute vorticity at 850 mb (η), relative humidity at 600 mb (H), the MPI wind speed (V_{pot}) based on the theory of Emanuel (1995), the 850 to 200 mb wind shear (V_{shear}), and GP[1] is proportional to the number of storms per decade per unit

1. While Emanuel and Nolan (2004) used the variable I for the genesis parameter, we here change to the more common notation GP, as is also used by Camargo et al. (2007a,b).

square of latitude and longitude.

V_{pot} refers to the maximum theoretical wind speed at the 10 m level in a mature hurricane over a constant SST ocean. Certainly, V_{pot} is larger for environments we consider favorable for tropical cyclones, especially since it increases rapidly with SST (for a fixed atmospheric sounding). Admittedly though, it is not obvious why the maximum wind speed of a theoretical cyclone should be a specific indicator the likelihood of TC *formation*, especially since their structrues are so different at the genesis and mature stages. However, the difference between an existing cyclone's current intenstity and the local value of V_{pot} is the strongest predictor of future intensity change in the SHIPS statistical model for TC intensity forecasting in the North Atlantic and East Pacific basins (DeMaria and Kaplan 1999). Perhaps this relationship extends to non-developed (pre-genesis) systems as well.

Examples of the capability of *GP* to reproduce annual and regional variations of TC genesis are presented in Camargo et al. (2007a, see their Figs. 1-3). Much as the Gray index was used in earlier climate modeling studies to evaluate changes in the TC genesis frequency in simulated future environments (Ryan et al. 1992; Watterson et al. 1995; Royer et al. 1998), this new genesis index has been used to evaluate the degree to which regional changes in genesis frequency caused by El Niño are due to changes in each of the 4 parameters in (1.1) (Camargo et al. 2007a), to evaluate the relationships between simulated TC activities and *GP* in various climate model simulations of present-day climate (Camargo et al. 2007b), and to estimate expected changes in genesis frequency in the simulated future environments of global climate models (Vecchi and Soden 2007).

While the earliest theories suggested that TC genesis occurs due to a fundamental instability of the tropical atmosphere to small perturbations (Charney and Eliassen 1964; Ooyama 1964),

the widely-held view has evolved to the idea that TC genesis can be thought of as a "finite-amplitude" instability, in that a pre-existing disturbance of some strength, such as a monsoon depression, easterly wave, mesoscale convective complex, or even a baroclinic cyclone is required for genesis (McBride 1981; McBride and Zehr 1981; Frank 1987; Rotunno and Emanuel 1987; Emanuel 1989). Our working hypothesis is that an increase of any of the four terms in (1.1) indicates a decrease in the size, coherence, or strength of an initial disturbance required to make the transition to a tropical cyclone before decaying or being disrupted by the synoptic environment. To reduce the space of parameters, and to avoid the complications of attempting to generate environments of RCE with both rotation and shear, in this paper we consider only environments with no mean wind shear. As we shall see, this will have significant consequences for our working hypothesis.

Section 2 documents the numerical model, parameterizations, and design of the simulations. Properties of the RCE environments, and their implicatons for the frequency of tropical cyclogenesis, are presented in Section 3. Section 4 describes tropical cyclogenesis in RCE from weak initial vortices, and Section 5 describes genesis from random convection. Conclusions are presented in Section 6.

2. Model, Parameterizations, and Simulation Design

a. Model and parameterizations

The atmospheric model used for this study is version 2.1.2 of the Weather Research and Forecast Model (WRF). WRF is a fully-compressible model of the atmosphere designed for mesoscale and convective-scale simulations of real-case and idealized weather phenomena (Skamarock et al. 2005).

The domain for all simulations is a square with doubly periodic boundary conditions. The

grid spacing is 4 km in the north and south directions, with 40 vertical levels. These levels are equally spaced in η coordinates, and thus are stretched in height, with 10 levels in the lowest 2.2 km. The model top is defined by pressure but sits at approximately 20 km altitude. The advective time step is 30 s, with 6 acoustic steps for each advective step.

Parameterizations for unresolved physical processes that are available with WRF 2.1.2 are used, all of which are closely related to commonly used schemes for research and numerical weather prediction. For microphysics, the WRF Single-Moment (WSM) 6-class scheme (with graupel) is used (Hong and Lim 2006). For the planetary boundary layer, we use the Yonsei University (YSU) scheme (Noh et al. 2003), which is an advancement of the Medium Range Forecast (MRF) scheme of Hong et al. (1996). The sophisticated Rapid Radiative Transfer Model (RRTM) scheme is used for long-wave radiation (Mlawer et al. 1997; Iacono et al. 2000).

There is no parameterization for shortwave radiation. Rather, the effects of ozone-related heating and the generation of the tropopause are simulated by the use of a relaxation scheme on the upper-level temperatures. Above z = 15 km, the atmosphere is relaxed to an isothermal profile with a relaxation time scale of 5 days. At each column in the model, the relaxation temperature is determined every 15 minutes from the mean temperature in the levels above 15 km. This allows the model to freely determine the tropopause temperature, based on the intensity of the simulated convection which is pushing into the upper troposphere.

In a doubly periodic domain with rotation, it is not physically consistent to include either a mean wind or a mean wind shear which is constant throughout the domain. Mean wind shear requires gradients of temperature and pressure which then cannot fulfill the periodic conditions. Combinations of mean wind and/or mean wind shear in doubly periodic domains have been created in previous studies by adding forcing terms to the equations of motion to relax the domain-

averaged winds to the desired state (e.g., Robe and Emanuel 2001; Tompkins 2001; Bretherton 2005).

However, as will be shown below, RCE without a mean surface wind produces an atmosphere with extremely high values of V_{pot} and is otherwise problematic. To adjust for this, we simulate the presence of a mean surface wind by modifying the wind speed used in the calculation of the surface evaporation rate as follows:

$$|V^*| = \left|\vec{\mathbf{v}} + u_m \hat{i}\right| \tag{2.1}$$

where $\vec{\mathbf{v}}$ is the 10 m surface wind and u_m is the speed of a mean "westerly" wind. The inclusion of a directional aspect of the mean surface wind reproduces the asymmetric patterns of surface fluxes and convection that would be expected with a developing cyclone.

b. Discussion of model and parameterizations

In this section we discuss some of the parameter choices which would seem to have the most significant effect on our results and their interpretation.

(1) Resolution

In recent years, a large number of studies have shown the significantly improved realism of tropical cyclone simulations that use sufficiently small grid spacings to be considered "cloud-resolving" and thus avoid the use of convective parameterizations. While earlier cloud-resolving simulations showed realistic dynamics using resolutions of 5-6 km (Liu et al., 1997; Frank and Ritchie 2001; Wang 2002), the apparent realism of the inner-core processes has increased steadily as the grid spacing has been further decreased from 5 to 3 to 1.67 km (e.g., Davis and Bosart 2002; Braun 2002; Rogers et al. 2003; Romine and Wilhelmson 2006). For genesis, cloud-resolving resolutions are perhaps even more important, due to the important roles of downdrafts and mid-level entrainment in delaying the genesis process (Rotunno and Emanuel 1987; Bister and

Emanuel 1997; Nolan 2007), and the role of small-scale vorticity dynamics in promoting it (Hendricks et al. 2004; Montgomery et al. 2006).

Unfortunately, the desire for the highest resolution possible must be balanced against the limitations of computer power and memory. Since this study requires the use of a large number of long simulations over large domains, resolutions on the order of 1-2 km were not feasible. In a study of the resolution dependence of simulations of RCE, Pauluis and Garner (2006) found that 4 km resolution produced results very similar to 2 km resolution, with the 4km resolution soundings having a warm bias of about 0.1K, and a water vapor bias of at most -2% at the top of the boundary layer. Given a review of the literature on RCE and on tropical cyclone simulations, and our own evaluations, we believe 4 km resolution allows for reasonably realistic simulations of convection and cyclogenesis while making the best use of computational resources.

(2) Shortwave radiation

In the energetic and dynamical balances of the tropical atmosphere, shortwave radiation has three major effects. First, it supplies heat energy to the ocean; second, stratospheric heating by absorption of ultraviolet light by ozone creates the tropopause; and third, there is some degree of clear-sky heating in the troposphere, mostly through direct absorption by water vapor (Wallace and Hobbs 2006). In our simulations the SST is held fixed, so the energy of short-wave radiation is not needed at the surface, and the upper-level relaxation scheme creates an isothermal layer which is similar to the real tropopause. Thus, the primary difference between our simulations and those with interactive shortwave radiation is the absence of clear-sky heating in the troposphere and its horizontal variations due to cloud albedo.

The neglect of a shortwave radiation parameterization has a number of benefits. It eliminates the need for consideration of a number of external factors, such as the seasonal and latitudi-

nal variations of the declination of the sun. It also eliminates the diurnal cycle, so that daily averages of the model output are not biased by the time of day. Finally, since the height of the tropopause is strongly influenced by heating from the absoprtion of ultraviolet light by ozone, the isothermal relaxation schemes allows this height to be more directly controlled by the intensity of the simulated convection, rather than by observed ozone profiles which are coded into most short-wave parameterizations (and which vary with latitude and season as well). Despite the arbitrary choice of the altitude above which the relaxation is enforced (z = 15 km), the relaxation scheme gives some freedom to the height of the tropopause. This will be shown below.

(3) The absence of wind shear

Unquestionably, vertical shear of the horizontal wind has an enormous impact on TC genesis and intensification (Gray 1968; Merrill 1988; DeMaria 1996; Frank and Ritchie 2001). While even the most active regions for TC genesis have seasonal mean shear values of about 10 ms^{-1}, many instances of TC genesis occur at times and locations that have very low shear due to the synoptic evolution of the upper-level environment (McBride and Zehr 1981; Frank 1987; DeMaria 2001). The study by Kaplan and DeMaria (2003) on rapidly intensifying TCs suggests that the effects of a small amount of shear in these favorable environments is quite similar to absolutely no shear. They found that the ratio of rapidly-intensifying versus non-rapidly-intesifying cases was nearly identical (about 3 to 1) in cases with 0-2 ms^{-1} and 2-4 ms^{-1} of 850 to 200 hPa wind shear (see their Fig 7a). This ratio decreased rapidly as shear increased above 4 ms^{-1}.

Thus, we view our "no-shear" environments as similar in terms of TC genesis favorability to "very low shear" environments. Our results will show that for more favorable environments, a developing disturbance needs less time to make the transition to a TC, suggesting that TC genesis would be more likely during a synoptically favorable (low shear) period of time.

c. Simulation design

The first step in the study of the "climate" associated with particular choices for SST, f, and u_m is the establishment of RCE in the model domain. To save computing time, RCE is always first achieved on a small domain, 200km x 200 km in size. The initial condition for each small-domain simulation is a hydrostatically balanced atmosphere with a temperature profile that begins at 2.5 K below the SST, and then decreases at a constant lapse rate of 6 K km^{-1}. The RH is set to 50% below z = 12 km, and 0% above. To initiate convection, random perturbations with root-mean-square variance of 0.1 K are added to the initial temperature field at each grid point below z = 3 km.

When the domain averaged-profiles of temperature and relative humidity (RH) reach a statistically steady state, the resulting profiles are used for two purposes. First, values of $V_{\rm pot}$, genesis index *GP*, and convective available potential energy (CAPE) are computed based on the sounding and the underlying SST. Second, the mean profiles are used as initial conditions for simulations with larger domains. These large-domain simulations are of two types: simulations of cyclogenesis from weak, balanced vortices, and simulations of spontaneous cyclogenesis from random convection. Details of the large-domain simulations are discussed further below.

3. Results of Small-Domain Simulations

a. Evolution to RCE

As found by Tompkins and Craig (1998b), it typically takes at least 50 days for random convection in an idealized, cloud-resolving model to achieve RCE. Fig. 1a shows the time evolution of the domain-averaged, frozen moist static energy (Bretherton et al. 2005),

$$h_f = c_p T + gz + Lq_v - L_f q_{ice} \tag{3.1}$$

for a small-domain, RCE simulation with SST = 27.5°C, f = 5.0x10^{-5} s^{-1}, and u_m = 3.0 ms^{-1}. A

steady equilibrium is not achieved until after 55 days. For this reason, all small-domain RCE simulations are integrated to 90 days, and the mean profiles are determined from domain-wide averages of the daily model output over the last 30 days.

Also shown in Fig. 1 are snapshots of the vertical velocity at z = 5 km, the equivalent potential temperature θ_e at the lowest model level (mean altitude about 100m), and the water vapor path (WVP) after RCE has been achieved. The RCE state is characterized by a small number of isolated, strong updrafts which are quasi-randomly distributed around the domain. However, a smoother but more widespread variability can be seen in the plots of θ_e and WVP. A few cold pools (indicated by low values of θ_e) and one significant dry region (indicated by low values of WVP) can be seen.

b. Aggregation

The atmospheric state that one might imagine for RCE in a three-dimensional, cloud-resolving model is much like the sporadic, seemingly random convection shown in Fig. 1. Recent studies have found that for some parameters and parameterizations, the equilibrium state for RCE is not one of random convection, but rather one defined by one or more large (100-400 km) clusters of moist convection surrounded by much drier areas with mean descending motion (Tompkins and Craig 1998a; Tompkins 2001; Bretherton et al. 2005). This "aggregation" is caused by a radiative-convective feedback, whereby upward motions are enhanced in regions of above average moisture and cloudiness, leading to further convection, while downward motions are enhanced in the drier regions, suppressing convection. Downdrafts, wind gusts, and their resulting increases in surface fluxes in the region of enhanced convection was also found to be critical to the aggregation process by further increasing convection in the active region. By replacing shortwave and longwave radiation parameterizations with horizontally constant radiative cooling,

Tompkins (2001) showed that some degree of aggregation can occur even without radiative feedbacks, due to the positive moisture feedback caused by the decreased effects of dry entrainment for cumulus updrafts in regions with greater mid-level humidity; however, similar modifications were found to eliminate aggregation by Bretherton et al. (2005), as did homogenizing the surface fluxes. Our simulations with interactive longwave radiation, but no shortwave radiation, lie somewhere between the extremes in radiative interaction defined by the Tompkins (2001a,b) and the Bretherton et al. (2005) studies.

To date, the majority of our simulations of RCE with no mean surface wind ($u_m = 0$) also show aggregation. While Bretherton et al. (2005) did not observe aggregation for domain sizes less than 384km x 384km (using 3km horizontal resolution), we have observed aggregation in domains as small as 160km x 160km. Our neglect of short-wave radiation in favor of the upper-level thermal relaxation scheme, and other differences in our parameterizations, may explain this discrepancy, but we will not explore this issue further here.

An interesting result from our small-domain simulations is that the inclusion of the mean surface wind suppresses the aggregation phenomenon. For all values of SST and f, aggregation did not occur for $u_m \geq 2$ ms^{-1}, and for most values, it was not seen for $u_m = 1$ ms^{-1}. Increasing the mean surface wind throughout the domain diminishes the relative value of the increased surface fluxes due to increased surface winds ("gustiness") in the convectively active region, which may explain this effect. However, as will be shown below, aggregation does occur in larger-domain simulations with $u_m = 3$ ms^{-1}.

c. Results for varying model parameters

To begin, we consider RCE simulations for SST = 25, 27.5, and 30°C, with $f = 5.0 \times 10^{-5}$ s^{-1} and $u_m = 3.0$ ms^{-1}. Mean profiles of temperature and RH are shown for these three cases in

Fig. 2. First, the temperature sounding shifts to warmer temperatures for larger SST, and this shift is slightly larger at higher altitudes, as the equilibrium soundings are very close to moist adiabats. Second, the altitude where the profile changes to isothermal, marking the height of the tropopause, also increases with SST. Third, mid-level relative humidity (RH) also increases with SST, by a significant amount between SST = 25°C and 27.5°C, and then only a small additional amount from SST = 27.5°C to 30°C. The changes in the RH profiles can also be seen as an upward shift in each case, as is evident from comparing the profiles in the upper-troposphere.

The environment with SST = 27.5°C, $f = 5.0\text{x}10^{-5}$ s^{-1}, and $u_m = 3$ ms^{-1} will hereafter be referred to as the control case, and we will vary the environmental parameters independently around these values.

The thermodynamic properties of the RCE soundings as a function of SST and f are summarized in Table 1. The numbers in each table entry are, respectively, the CAPE (J kg^{-1}), the maximum potential intensity (V_{pot}, ms^{-1}), and the genesis index GP as defined in (1.1). GP is computed with $V_{\text{shear}} = 0$. CAPE is computed for undiluted parcels lifted from the lowest model level (at about z = 100 m). For the parameter σ, which defines the extent to which the moist convection is reversible (σ =0) or pseudoadiabatic (σ = 1), we chose the compromise value σ = 0.5, since a mixture of both processes occurs in the simulations. For V_{pot}, we use the MPI theory of Emanuel (1995), without the dissipative heating correction of Bister and Emanuel (2002), since the model does not have dissipative heating. For the ratio of enthalpy exchange to momentum exchange coefficients, we use $C_k/C_d = 0.5$, as this was representative of the ratio generated underneath the eyewalls of the model-simulated hurricanes.[2]

According to Table 1, V_{pot} increases by about 10% as the SST increases from 25 to 30°C. This increase is substantially smaller than would be normally be associated with such an SST

change, but this is due to the fact that the atmosphere has adjusted to a state of RCE with the ocean temperature. *GP* increases with SST as well, but the increase in *GP* is even greater than the corresponding increase in V_{pot} would suggest. This is due to an increase in the 600 mb RH, as shown in Fig. 2b (the height of the 600mb level is near $z = 4$ km for all simulations). The value of the Coriolis parameter has only small effects on V_{pot} and CAPE, with very small decreases found in each as f increases from 2.5 to 7.5×10^{-5} s^{-1}. There is a substantial increase in *GP*, of course, since the environmental vorticity η in (1.1) is equal to f. It is worth noting that the values of *GP* for the control case and for SST = $30°C$ are quite similar to the peak values of *GP* in the Northern Hemisphere for September. However, this is probably due to a compensation for the lack of wind shear by underestimation of V_{pot} due to the low values of C_k/C_d in the model.

Now setting SST = $27.5°C$ and $f = 5.0 \times 10^{-5}$ s^{-1}, we show in Fig. 3 soundings generated with different values of mean surface wind u_m. Remarkably, the changes in the soundings as u_m increases from 1 to 5 ms^{-1} are much more profound than the changes as SST varies from 25 to $30°C$. As u_m increases, the atmospheric temperature and the mid-level humidity both increase significantly. Table 2 shows more data for RCE simulations with $f = 5.0 \times 10^{-5}$ s^{-1} but for varying values of SST and u_m. As u_m increases, the MPI for each sounding decreases, while CAPE increases substantially. The increase in CAPE is due to increased moistening of the boundary layer by increased surface fluxes, while the decrease in MPI is due to increased warming aloft by deeper and moister convection. Interestingly, *GP* responds to increasing u_m by first increasing

2. The surface layer parameterization used for this study contains the standard Charnok (1955) relationship between surface roughness and wind speed, which leads to increasing values of C_d at high wind speeds, and values of C_k/C_d decreasing to 0.5 or less underneath the eyewalls of the simulated storms. Since TC genesis occurs when wind speeds are low, one could argue that a lower value of C_k/C_d should be used for the calculation of V_{pot} and GP. Indeed, $C_k/C_d=1$ was used in the development of the empirical parameters in GP. Using this ratio simply increases all the values of V_{pot} by about 40%, and increases the values of GP considerably. However, we have chosen to use values of C_k/C_d (and thus V_{pot}) which are consistent with the present model, and the results that follow and their interpretation are otherwise unchanged.

due to the increased mid-level humidity, but then decreasing due to decreasing V_{pot}.

4. TC Genesis from Weak Initial Vortices

a. Domain, soundings, and initial conditions

In the results that follow, a weak, balanced vortex is introduced into a much larger 1200x1200 km domain, with an initial atmospheric sounding that is the mean RCE state generated by a small-domain simulation with the same values of SST, f, and u_m.

The balancing scheme described in Nolan et al. (2001) is used to initialize the model with an axisymmetric vortex with a prescribed azimuthal wind field $V(r, z)$. An azimuthal wind profile is first computed from radial integration[3] of a Gaussian vorticity profile

$$v_0(r) = \frac{1}{r}\int_0^r r\zeta dr, \tag{4.1}$$

where ζ is the relative vertical vorticity and is defined to be

$$\zeta(r) = A\exp\left\{-\left(\frac{r}{b}\right)^2\right\}. \tag{4.2}$$

Since the total circulation must be zero in a doubly periodic domain, the velocity profile is forced to go smoothly to zero across some radius R as:

$$v_s(r) = v_0(r) \times \exp\left\{-\left(\frac{r}{R}\right)^6\right\} \tag{4.3}$$

Finally, the wind profile is extended into the vertical with the following form:

$$V(r, z) = v_s(r) \times \exp\left\{-\frac{\left|z - z_{\max}\right|^{\alpha}}{\alpha L_z^{\alpha}}\right\} \tag{4.4}$$

3. The velocity profile from integration of a Gaussian vorticity profile has an exact solution, but the calculation is performed numerically since the vortex generation code is designed to work for arbitrary vorticity profiles.

where L_z indicates the depth of a low-level baroptropic part of the vortex, α is the decay rate with height above and below the barotropic zone, and z_{max} is the altitude of the maximum cyclonic wind speed.

For most of the simulations, the parameters A and b are chosen to define a vortex with a radius of maximum winds RMW = 100 km and maximum initial cyclonic wind speed v_{max} = 5 ms^{-1}. These maximum winds are set at an elevation z_{max} = 3720 m, such that the circulation is a weakly baroclinic, mid-level vortex which is representative of the precursor disturbances which most often lead to TC genesis in the real atmosphere, such as monsoon depressions, mesoscale convective vortices (MCVs) and easterly waves (McBride 1981; McBride and Zehr 1981; Frank 1987), all of which are "cold-core" cyclones in the lower troposphere. The parameters L_z = 3175.23 m and α = 2.0 are chosen so that the maximum surface wind speed is exactly half (2.5 ms^{-1}) of the wind speed at z_{max}. The outer wind field is smoothed to zero across R = 350 km as in (4.3). This initial azimuthal wind field is shown in Fig. 4.

As in the small-domain simulations, random perturbations were added to the temperature field below 3 km throughout the domain. In this way, the developing vortex must "compete" with convection throughout the domain for moisture and energy.

b. Main results

Even in environments very ideal for genesis, simulated vortices of this type have been found to go through a slow development process before arriving at a period of rapid intensification (Ooyama 1969; Rotunno and Emanuel 1987; Persing and Montgomery 2003; Nolan 2007). During this development, the inner core of the vortex slowly becomes saturated due to sporadic convection, while the vortex intensifies in the mid-levels. Once the inner core is saturated, the inner-core convection becomes stronger and more persistent, and a smaller-scale vortex rapidly

develops near the surface.

As examples of this process, and to show the sensitivity of the genesis process to the environment, we show in Fig. 5a the time evolution of the maximum 10 m winds in simulations of genesis from initial vortices with v_{max} = 5.0 ms^{-1} and RMW = 100 km, for the control case and for SST = 25 and 30°C. These plots are quite noisy, since no distinction is made between gusts due to local convection and the mean circulation around the vortex. There is little difference in the trends of the three curves until about t = 2.2 days, when surface winds for the warmer SSTs start to increase quite a bit more quickly than for the cooler SSTs.

Three time series of maximum wind are shown for the control case (labelled as a, b, and c in Fig. 5a). These are the results of three identical simulations with different random noise in the initial temperature fields. The closeness of the three curves during the genesis and rapid intensification stages shows that the time to genesis is not dependent on the random initial state, but is strongly controlled by the initial vortex and the environment.

The distinctions in the timing and rate of development can be seen a little more clearly in the evolution of the minimum surface pressure, as shown in Fig. 5b (again with three curves for the control case). All three cases show the beginnings of a decline in surface pressure around t = 1.5 days. However, the minimum pressures for the warmer SSTs begin to fall much more rapidly than for SST = 25°C, and after t = 2.5 days the pressure fall for SST = 30°C becomes much more rapid than for SST = 27.5°C.

Considering the significant differences in SST involved, it is a bit surprising that the beginning of the steady pressure fall occurs at nearly the same time for all three simulations. However, while the SST differences are large, the overlying atmospheres are in equilibrium with these temperatures, and so the value of V_{pot} increases from 63.8 ms^{-1} for 25°C to only 70.6 ms^{-1}

for $30°C$ - a change of only about 10%. With this in mind, the seemingly small differences in the rate of development make more sense.

A clearer picture of the differences in the genesis and development of these three cyclones can be seen by incorporating the radial structure of the evolving vortices into the analysis. Fig. 6 shows Hövmoller diagrams of the azimuthally averaged azimuthal 10 m wind field for the three different SSTs. The wind speeds have been normalized by V_{pot} for each case. The contraction and then rapid intensification of the surface vortex occurs about 12 hours earlier for $27.5°C$ than for $25°C$, and another 8 hours earlier for $30°C$ than for $27.5°C$. For example, the 4th contour in each plot indicates a ratio of V/V_{pot} of 0.32, and this value first appears at t = 3.1 days, 2.7 days, and 2.5 days for SST = 25.0, 27.5, and $30.0°C$, respectively.

An even more robust picture of the differences in genesis is seen in Hövmoller diagrams of the vertical component of the vorticity vector (hereafter, vertical vorticity) at z = 2 km and the vertical velocity at z = 5 km, as presented in Fig. 7. The vorticities are normalized by f, while the vertical velocities are normalized by V_{pot}. All three cyclones show little development for the first 24 hours, but then each vortex develops a wide, somewhat noisy region of low-level vorticity, which then contracts and intensifies. Just after this contraction, the vertical velocity field shows that each vortex develops a coherent eyewall, as indicated by the appearance of a distinct inner-core maximum in the vertical velocity. The coherence and intensity of the eyewalls are quite different between the three simulations, with the warmer SST, higher V_{pot} simulations showing a more coherent and more intense inner core, developing at earlier times in each case.

c. Measures of "genesis time"

For a more quantitative analysis of the previous results, it would seem desirable to have a precise definition of the time of TC genesis. We attempted to conceive an objective definition of

the "time to genesis" for these simulations. One definition considered was simply the time when either the maximum surface wind speed or the maximum azimuthally averaged surface wind speed reached certain values. However, due to the noisiness of both these curves, the genesis time was often not clearly defined, with differences of only 6-12 hours found between many of the simulations. Normalization by V_{pot} made this definition even less distinctive.

Another definition we considered was based on the development of a low-level vortex that is stronger than the original mid-level vortex, defining genesis to occur when the peak value of the azimuthally averaged wind or vorticity at some low altitude exceeds that at some higher altitude. Unfortunately, this did not produce consistent results either. In some cases, the low-level mean vorticity never exceeded vorticity values of those at higher altitudes until very late into the intensification stage; in others, upper and lower level values of vorticity crossed each other more than once.

The minimum surface pressure and its rate of fall were also considered. While in some cases there was a distinct increase in the rate of pressure fall at specific times (e.g., Fig. 5b, solid curve), in others there were no such clear indicators (e.g., Fig. 8b, solid curve). However, we found that a self-consistent way to normalize the rate of pressure fall was to compare it to the largest rate of pressure fall during the period of most rapid intensification. Through trial and error, we found that a useful and fairly consistent "genesis time" could be defined as the first time the 8 hour pressure fall reached a rate equal to 25% of the fastest pressure fall. Since the model data was saved only every 4 hours for most of these simulations, the minimum surface pressure data was interpolated to 1-hour data points using cubic spline interpolation, and then the 8 hour pressure falls were computed and compared. This allows the genesis time to occur at times not necessarily divisible by 4 hours.

Objective genesis times for all the initial-vortex simulations are presented in Table 3. Also included are the time of the fastest 8 hour pressure fall. This "time of most rapid intensification," while perhaps not directly related to "genesis" of the cyclone, helps to differentiate the rates of TC development among the various cases. The time of fastest pressure fall was also consistently close to subjective genesis times based on the authors' interpretations of the formation of the inner core as illustrated by the Hövmoller diagrams of vertical velocity and vorticity.

d. A note on maximum intensity

The model simulations each peak in intensity about 10% short of their respective V_{pot} values. For example, the simulations shown in Fig. 5a reach wind speeds of 56, 59, and 64 ms^{-1}, while their corresponding V_{pot} values are 63.8, 66.9, and 70.6 ms^{-1} (see Table 1). This "failure" to reach MPI could be due to a number of reasons. The V_{pot} calculation is highly sensitive to some tunable parameters, the values of which are only broadly representative of the model simulations. Another reason these cyclones do not reach, nor sustain, their MPI is the relatively small size of the domain. As they reach significant intensity, the cyclones "fill up" the upper levels of the domain with heat and moisture. This modification of the upper environment halts and ultimately reverses the intensification of the cyclones.

e. Main results, continued

Fig. 8 shows wind and pressure data for the control simulation and for simulations with f = 2.5 and 7.5×10^{-5} s^{-1}. The high f simulation appears to begin some development (in terms of pressure) after only 18 hours, while a consistent pressure fall does not begin for the low f simulation until 2 days have passed. However, the velocity increase and pressure fall during the "rapid intensification" phase of development is quite similar for all three storms, with the $f = 5.0 \times 10^{-5}$ s^{-1} simulation actually intensifying faster than the other two. Objective genesis times based on the rates of pressure fall are 54, 42, and 68 hours for f = 2.5, 5.0, and 7.5×10^{-5} s^{-1}, respectively. A more dis-

tinct trend in genesis time can be seen from the comparing the Hövmoller diagrams of vertical velocity and vorticity for these three cases (Fig. 8c,d). A coherent vorticity core and eyewall feature appears *sooner* for the low *f* case than for the other two simulations. This result is consistent with the dimensional analysis and simulations of Emanuel (1989, see Table 1 of that paper). Since the natural length scale is inversely proportional to *f*, the same initial vortex in a lower-*f* environment develops and intensifies more quickly, since it is smaller in a non-dimensional sense. Similarly, the slower pace of intensification for the high *f* case is consistent with this scaling.

The low *f* cyclone seems to experience a disruption of its intensification around $t = 4$ days. Due to the very low inertial stability of its environment, this cyclone contracts to an extremely small size, such that the inner core cannot be well-resolved by the model (not shown). Regardless of the precise reason for the disruption in the low *f* case, these simulations with varying *f* do not indicate a clear trend in genesis time, certainly not in the direction that the changes in *GP* would suggest (*GP* = 13, 35, and 66 for these three cases), and possibly in the opposite direction for development from a pre-existing vortex.

The mean surface wind, u_m was found to have significant effects on V_{pot} and *GP*. While V_{pot} decreased montonically with increasing u_m, *GP* increased as u_m increased from 1 to 3 ms^{-1}, but then decreased for higher values of u_m (see Table 2). Is this trend in *GP* correlated with decreasing times to genesis in the initial-vortex simulations? In fact, it is not. Fig. 9 shows maximum surface winds and minimum surface pressure for the control simulation and for values of u_m = 1 and 5 ms^{-1}, along with Hövmoller plots for vorticity and vertical velocity for the same simulations. Genesis and rapid development occurs more quickly for u_m = 1 ms^{-1} than for 3 ms^{-1}, and sooner for 3 ms^{-1} than for 5 ms^{-1}. As shown in Table 2, the values of *GP* for u_m = 1 and 5 ms^{-1} are about the same (22,23), while for u_m = 3 ms^{-1} *GP* is much larger (35). Nonetheless, the speed of

development follows the trend in V_{pot}, with (objective) genesis occurring at t = 36 h for u_m = 1 ms^{-1} (V_{pot} = 83.7 ms^{-1}), t = 42 h for u_m = 3 ms^{-1} (V_{pot} = 66.9 ms^{-1}), and t = 70 h for u_m = 5 ms^{-1} (V_{pot} = 55.6 ms^{-1}).

f. Discussion

Given the ability of *GP* to reproduce regional and seasonal variability of TC genesis (Emanuel and Nolan 2004; Camargo et al. 2007a), the inconsistencies between the trends in *GP* and the rates of TC development shown above are surprising. There could be several reasons for the discrepancies. First, our interpretation of the time to genesis for a pre-existing vortex as an equivalent indicator of the likelihood of TC genesis may be incorrect. Rather, *GP* may be more indicative of the favorability of the environment to form and support the pre-cursor disturbances that go on to become TCs, while the rate of development in the "second stage" of genesis may be more closely correlated with V_{pot}.

A second and more daunting possibility is that the expression of *GP* as separable functions of the environmental parameters may simply not be valid. For example, regarding the effects of mid-level humdity, one of the early explanations for the negative effects of vertical wind shear is that the winds aloft transport heat and moisture generated by convection away from the low-level center (Simpson and Riehl 1958; Gray 1968). If this is true, then the environmental air that replaces this moisture would have a large impact on the future development of the cyclone. In the absence of shear, this process might not occur, and it may be that the convection can very quickly saturate the inner core with little influence from the environment. Thus, the relative effects of environmental mid-level humidity may vary in relation to the wind shear. Conceivably, this could also be true for the Coriolis parameter - that higher values of f allow weaker cyclones to achieve genesis in the presence of wind shear. Only further research can answer these questions.

g. Results for weaker vortices and for lower SSTs

The working hypothesis outlined in Section 1b proposes that there is a finite amplitude threshold size or strength necessary for a disturbance to achieve TC genesis, and that this threshold decreases as *GP* increases. For a given RCE environment, we would expect to find an initial vortex amplitude below which TC genesis fails to occur. Fig. 10 shows time series of minimum surface pressure for the "control" initial-vortex simulation with $v_{\max} = 5$ ms^{-1}, and for two additional simulations with $v_{\max} = 2.5$ and 1.25 ms^{-1} (corresponding to maximum initial surface winds of 1.25 and 0.6125 ms^{-1}, respectively). Genesis is significantly delayed for the weaker vortices, with the $v_{max} = 2.5$ ms^{-1} simulation not showing significant development until 7 days, and the $v_{\max} = 1.25$ ms^{-1} simulation not showing development until 9 days. Nonetheless, TC genesis does occur for these extremely weak vortices. Contrary to our working hypothesis, there seems to be no lower limit on the strength of the initial vortex needed for genesis, suggesting that in RCE without shear TCs might be able to form without a pre-existing vortex whatsoever. As we will show in the next section, this is indeed the case (at least for this model and its parameterizations).

We also performed a number of initial vortex simulations with substantially colder temperatures, such as for SST = $20°C$ and $10°C$. We found that TC genesis occurred in every case - although for the colder temperatures, the TCs generated were broad and quite weak (consistent with V_{pot} for each case). Above freezing temperatures and in the absence of wind shear, there does not appear to be a critical temperature below which TC genesis from finite initial perturbations cannot be supported.

5. Spontaneous Cyclogenesis

a. Initialization and results

To further investigate whether tropical cyclogenesis might occur without the benefit of a

pre-existing circulation, we performed a number of longer simulations of RCE on larger domains. As before, these simulations were initialized with the RCE profiles generated by small-domain simulations, and random temperature perturbations were added to the resting initial state.

Simulations with a number of parameter choices have generated tropical cyclones from random convection. However, computational limitations, model error fixes, and our evolving understanding of the impact of the mean surface wind have prevented obtaining a consistent set of spontaneous genesis simulations across the parameter space defined by SST, f, and u_m. Some of the earlier spontaneous genesis results are summarized in Nolan et al. (2006). Bretherton et. al. (2005) also observed spontaneous genesis when they added sufficient rotation to their simulations of convective aggregation.

Rather than attempting to explore the environmental parameter space for spontaneous genesis simulations, we instead present a particular case of spontaneous genesis. The domain size is 1200kmx1200km, and the environmental parameters are the same as the control case above, with SST = 27.5°C , $f = 5.0\text{x}10^{-5}$ s^{-1}, and $u_m = 3$ ms^{-1}. Evolution of the maximum surface winds and minimum surface pressure are shown Fig. 11. At $t = 8$ days, the maximum surface winds transition from a consistent value of just less than 10 ms^{-1} to around 15 ms^{-1}. At this time, the surface pressure trend changes from essentially flat to having an almost impercetibly slow decrease, with a more obvious decline beginning after 12 days. Using the objective measures of TC development described above, TC genesis occurs at 364 hours (15.2 days), and the most rapid intensification occurs at 404 hours (16.8 days).

The randomness of this convection can be seen in Fig. 12a, which shows the water vapor path (WVP, in mm) in each model column at $t = 4$ days. At this time there is no discernable pattern to the moisture field. The subsequent panels show WVP at $t = 6$, 8, and 10 days. At 6 days,

regions of moderate drying have appeared in the top-center, lower-right, and lower-left parts of the domain, while the WVP has become slightly enhanced in the upper-right and upper-left quadrants. At day 8, the drying regions have expanded and become significantly drier, while the enhanced WVP region seems to have coalesced into a large clump of increased moisture in the middle-right side of the domain, continuing across the right boundary to the left side. This coalescence around day 8 is coincident with the jump in maximum surface winds and the beginning of the very slow pressure fall shown in Fig. 11. By day 10, the organization of moisture into a large rotating patch is clearly underway. Thus, the moisture field suggests a slow and steady organization over period of about 4 days.

The dynamical fields indicate TC genesis occurring later in the simulation and at a slightly faster rate. This is illustrated in terms of the vertical vorticity at z = 2.2 km as shown in Fig. 13 at t = 11, 12, 13, and 14 days. At 11 days, the vorticity appears quite disorganized, but there are two areas of enhanced vorticity, one centered near x = 700 km, y = 300 km and the other around x = 550 km, y = 1000 km. At day 12, the lower-right region seems to have developed a ring of larger (both negative and positive) vorticity anomalies, while the upper-left activity has declined. At t = 13 days, the vorticity in the lower-right region has again coalesced into a broad region of increased (positive) vorticity with embedded higher positive and negative anomalies, and some spiral features to the north and west. At t = 14 days, this broad area of enhanced positive vorticity has coalesced into a smaller region of positive vorticity, with a cluster of higher vorticity anomalies at its center. One day later this vorticity center is a steadily intensifying tropical cyclone (not shown).

b. Large-scale evolution leading to small-scale genesis

The moisture and vorticity fields shown above suggest that spontaneous TC genesis in this

simulation is a process with two stages. The first stage appears equivalent to the "aggregation" phenomenon previously described in section 3b, which involves a radiative-convective feedback, where by the more moist regions generate enhanced convection due to increased mid-level moisture and mean ascent due to decreased radiative cooling (as compared to the other regions). The second process is more like the TC genesis shown above, whereby a pre-existing circulation with embedded convection contracts into a TC.

Bretherton et al. (2005) demonstrated the radiative-convective feedback though a "quartile analysis" of the model fields, which we will now replicate. The model domain is divided into 400 equal-sized squares of size 60 km x 60 km. Mean values of WVP are computed for each square. The squares are sorted according to their values of WVP, and then values of WVP and other variables are averaged for the first quartile (first 100) of the squares, and then the next quartile, and so on. Note that all the fields are sorted by their WVP values, e.g., the first quartile data for vorticity is the mean of the vorticity in the squares with the top 100 values of WVP, not vorticity itself.

The results of this analysis, presented in Fig. 14, are similar to those of Bretherton et al. (2005). Over the first few days, WVP in the wettest quartile begins to slowly increase above the values in the second and third quartiles, due to both an increase in mean temperature and a small increase in humidity. WVP of the driest quartile decreases in a similar fashion. Between $t = 6$ and 8 days the first and second quartiles begin to separate more quickly from the drier quartiles.

Energy loss due to longwave radiation is nearly indistinguishable among the quartiles until $t = 4$ days, when the first and second quartiles begin to lose less energy than the third and fourth. This is the moist-radiative feedback at work. The outgoing radiation in two drier quartiles falls at first, but then increases for a few days before falling again significantly. This temporary increase is due to increased high cloudiness spreading out to the drier regions as deep convection increases

in area and intensity in the moist quartile during the aggregation phase.

The decreased radiative cooling in the moist region supports a weak mean vertical motion (w) punctuated by spikes of higher mean values associated with strong individual convective events. In a manner similar to WVP and w, the vorticity in the wettest quartile increases very slowly for the first 6 days, followed by an accelerated rise from 8 to 12 days. However, this rise in vorticity preceeds the formation of the TC between days 13 and 14 (as seen in Fig. 13). The fact that there is no additional jump in vertical vorticity during the genesis and rapid development of the cyclone indicates that there is a rearrangement of vorticity in the moist region at this stage, rather than an increased transport from the other regions.

The evaporation from the surface is nearly equal among the quartiles until day 6. At this time, the fluxes in all but the last quartile begin to increase. Between days 6 and 8, the top two quartiles separate from the bottom two, and after day 14, the top quartile value increases far beyond the other three. The increased evaporation in all the regions (as also indicated by the mean), followed by the larger increase in the moist region, suggests that a second feedback mechanism is occurring, whereby the increased low-level winds (with gustiness and downdrafts in the convecting region) is causing more evaporation, leading to more convection and stronger circulations. This feedback is more commonly known as wind-induced surface heat exchange (WISHE, see Yano and Emanuel 1991).

The quartile values for precipitation, however, do not follow this pattern shown by the vapor flux, with the top quartile exceeding the others from day 1 onward, and diverging to vastly larger values after day 8, after which precipitation in the other quartiles decreases to near zero. This disparity between precipitation and evaporation indicates, not surprisingly, that aggregation and TC genesis are associated with net transport of water from the dry to moist regions.

6. Conclusions

a. Summary

We have presented a new approach for studying the relationship between the likelihood (or frequency) of tropical cyclogenesis and the thermodynamics of the large-scale environment. We used a high-resolution, cloud-resolving, full-physics model of the atmosphere to first simulate environments of radiative-convective equilibrium (RCE), and then to simulate the genesis and rapid intensification of tropical cyclones in these environments. By using RCE as a background environment, we reduced the "space" of all possible thermodynamic environments to one which was uniquely determined by just three parameters: the SST, the mean surface wind, and the Coriolis parameter.

A first result from our investigations is that unsheared RCE is in fact a very favorable place for tropical cyclones to form. We found that TC genesis could occur from very weak initial vortices, and could occur even in atmospheres in RCE with very low SSTs. In a simulation with SST = 27.5°C and $f = 5.0\text{x}10^{-5}\text{s}^{-1}$, TC genesis occurred spontaneously from random convection.

Since TC genesis resulted from even the weakest vortices, we explored the ways in which changing the environmental parameters affected the *rate* at which a weak, mid-level vortex evolved to TC genesis and rapid development. The primary result of this paper is that the rate of development of the cyclone (and inversely, the "time to genesis") is highly correlated with the value of the maximum potential intensity (V_{pot}) as computed by the intensity theory of Emanuel (1995). Other factors, such as the mid-level RH and the Coriolis parameter, were found to have little impact on genesis time as compared to $V_{\text{pot.}}$ Since these other factors are important parts of the genesis index of Emanuel and Nolan (2004), the results here could indicate that the success of the genesis index (1.1) is dominated by the V_{pot} term (and of course the V_{shear} term), or that there

are compensating errors in the η and *H* terms. It is also possible that the likelihood (or frequency) of TC genesis, as indicated by the value of *GP*, is not so well correlated with the rate of TC genesis from a weak, mid-level vortex as we have presumed. Another more challenging possibility is that the influences of η and *H* in favoring or suppressing genesis are lost in an environment with little or no wind shear.

In contrast with the strong relationship between V_{pot} and genesis time, we found no relationship between CAPE and the rate of cyclone development. While environmental CAPE has been shown to have little bearing on TC intensity (Drury and Evans 1993; Persing and Montgomery 2005), this indicates it has little bearing on the likelihood of genesis as well. This suggests a fundamental flaw in genesis parameters based on instability, such as those of Gray (1968), DeMaria (2001), and to some extent the "convective" genesis parameter of Royer et al. (1998).

A case of spontaneous genesis from random convection was analyzed. Following in the work of Bretherton et al. (2005), we showed that the cyclone formation followed a two-stage process. The first stage is caused by a radiative, convective, and surface-gustiness feedback, whereby decreased outgoing longwave radiation in a region of enhanced moisture leads to warming, mean ascent, increased convection, and then increased moisture, and so on. A broad circulation develops in and around this region of enhanced moisture. In the second stage of development, the broad circulation contracts into a TC in a manner similar to the simulations with initial vortices, due to a WISHE feedback and the enhanced trapping of heat and energy released by convection as the local inertial stability increases (Hack and Schubert 1986; Nolan et al. 2007).

In section 3b, we reported that the mean surface wind prevented aggregation in the small-domain (200km x 200km) simulations. While the occurrence of the aggregation process on the larger domain (1200km x 1200km) unfortunately indicates yet another degree of model sensitivity

for RCE states, it is at least consistent with Bretherton et al. (2005), who also found that aggregation was suppressed on sufficiently small domains. One possible reason for a domain-size dependence is that there may be a fundamental length scale to the aggregating region which is both model and parameterization dependent; if this scale is larger than the domain size, aggregation may not be prevented. For example, the aggregating region shown in Fig. 12 would not fit inside one of our small-domain simulations. A full explanation of these relationships (domain size, mean surface wind, and aggregation) remains for future work.

b. Working hypothesis revisited

To what extent has the working hypothesis been supported by our results? Without a doubt, the results indicate that TC genesis is very highly correlated with V_{pot}, and not with SST independently. This correlation was measured by the (decreasing) time to genesis for a weak initial vortex as V_{pot} was increased, either by increasing SST or decreasing u_m. As *GP* increases rapidly with V_{pot}, this result supports an increase in the likelihood of TC genesis as *GP* increases. However, for genesis from a pre-existing vortex, we did *not* find a clear correlation between the time to genesis and the Coriolis parameter *f*, nor with mid-level RH (although this could not be varied independently from V_{pot}).

We also proposed that enivronmental parameters consistent with the tropics represent a region of "finite-amplitude instability," where disturbances below some threshold intensity will not develop into a TC. However, simulations with extremely weak initial vortices (v_{max} = 2.5, 1.25 ms^{-1}) ultimately did arrive at TC genesis. The extremely slow pace of the development (as compared to v_{max} = 5 ms^{-1}), and an examination of the evolution leading up to genesis in these cases (not shown), indicated that the genesis mechanism was more like the spontaneous genesis mechanism discussed in Section 5: the extremely weak initial vortex simply provides the seed

location for the aggregation process that leads to genesis. For unsheared RCE, our preconceived notion of a finite amplitude threshold for genesis may instead mark the division between the more "direct" genesis process illustrated by the control case and a longer-term genesis process driven by aggregation.

Unquestionably, the absence of wind shear in our simulations is the major limiting factor on the application of the present results to the real atmosphere and any questions of TC genesis and frequency in a changing climate. We are currently devising a method to incorporate mean wind and mean wind shear into our RCE atmospheres, and our investigations of TC genesis will resume with shear as a primary parameter of influence.

Acknowledgements

The authors would like to gratefully acknowledge Dr. Shu-Hua Chen for the development of codes to implement idealized initial conditions in WRF and the idealized tropopause relaxation scheme, and three anonymous reviewers for their valuable comments. This research was supported by the National Science Foundation under grant ATM-0432067.

References

Bengtsson, L., H. Bottger, and M. Kanamitsu, 1982: Simulation of hurricane-type vortices in a general circulation model. *Tellus*, **34**, 440-457.

Bengtsson, L., M. Botzet, and M. Esch, 1996: Will greenhous gas-induced warming over the next 50 years lead to higher frequency and greater intensity of hurricanes? *Tellus*, **48A**, 57-73.

Bengtsson, L., K. I. Hodges, M. Esch, N. Keenlyside, L. Kornblueh, J.-J. Luo, and T. Yamagata, 2007: How may tropical cyclones change in a warmer climate? *Tellus*, in press.

Bister, M., and K. A. Emanuel, 1997: The genesis of Hurricane Guillermo: TEXMEX analyses and a modeling study. *Mon. Wea. Rev.*, **125**, 2662-2682.

Braun, S. A., 2002: A cloud-resolving simulation of Hurricane Bob (1991): Storm structure and eyewall buoyancy. *Mon. Wea. Rev.*, **130**, 1573-1592.

Bretherton, C. S., P. N. Blossey, and M. Khairoutdinov, 2005: An energy-balance analysis of deep convective self-aggregation above uniform SST. *J. Atmos. Sci.*, **62**, 4273-4292.

Broccoli, A. J., and Manabe, S., 1990: Can existing climate models be used to study anthropogenic changes in tropical cyclone climate? *Geophys. Res. Lett.*, **17**, 1917-1920.

Byers, H. R., 1944: *General Meteorology.* McGraw-Hill, New York, 645 pp.

Bister, M., and K. A. Emanuel, 1997: The genesis of Hurricane Guillermo: TEXMEX analyses and a modeling study. *Mon. Wea. Rev.*, **125**, 2662-2682.

Bister, M., and K. A. Emanuel, 1998: Dissipative heating and hurricane intensity. *Meteor. Atmos. Phys.*, **65**, 233-240.

Camargo, S. J., K. A. Emanuel, and A. H. Sobel, 2007a: Use of a genesis potential index to diagnose ENSO effects on tropical cyclone genesis. *J. Climate*, in press.

Camargo, S. J., A. H. Sobel, A. G. Barnston, and K. A. Emanuel, 2007b: Tropical cyclone genesis potential index in climate models. *Tellus A*, **59**, 4428-443.

Charney, J. G., and A. Eliassen, 1964: On the growth of the hurricane depression. *J. Atmos. Sci.*, **21**, 68-75.

Charnok, H., 1955: Wind stress on a water surface. *Quart. J. Roy. Meteor. Soc.*, **81**, 639-640.

Chauvin, F., J.-F., Royer, and M. Deque, 2006: Response of hurricane-type vortices to global warming as simulated by ARPEGE-Climat at high resolution. *Climate Dynamics*, **27**, 377-399.

Davis, C., and L. F. Bosart, 2001: Numerical simulations of the genesis of Hurricane Diana (1984). Part I: Control simulation. *Mon. Wea. Rev.*, **130**, 1100-1124.

Davis, C., and L. F. Bosart, 2002: Numerical simulations of the genesis of Hurricane Diana (1984). Part II: Sensitivity of track and intensity prediction. *Mon. Wea. Rev.*, **130**, 1100-1124.

DeMaria, M, and J. Kaplan, 1999: An updated statistical hurricane intensity prediction scheme (SHIPS) for the Atlantic basin. *Wea. Forecast.*, **9**, 209-220.

Drury, S., and J.-L. Evans, 1993: Sea surface temperature and CAPE: Importance for tropical cyclone intensity. *Preprints, 20th Conf. on Hurricanes and Tropical Meteorology, San Antonio, TX*, Amer. Meteorol. Soc., 89-92.

Emanuel, K. A., 1988: The maximum intensity of hurricanes. *J. Atmos. Sci.*, **45**, 1142-1155.

Emanuel, K. A., 1989: The finite-amplitude nature of tropical cyclogenesis. *J. Atmos. Sci.*, **46**, 3431-3456.

Emanuel, K. A., 1995: Sensitivity of tropical cyclones to surface exchange coefficients and a revised steady-state model incorporating eye dynamics. *J. Atmos. Sci*., **52**, 3969-3976.

Emanuel, K. A., and D. S. Nolan, 2004: Tropical cyclones and the global climate system. *Preprints, 26th Conference on Hurricanes and Tropical Meteorology, Miami, Florida.*

Evans, J.-L., 1992: Comment on "Can existing climate models be used to study anthropogenic changes in tropical cyclone climate?" *Geophys. Res. Lett.*, **19**, 1523-1524.

Frank, W. M., 1987: Tropical cylone formation. *A Global View of Tropical Cyclones*. R. Elsberry et al. (eds). Naval Postgraduate School, Monterey, CA.

Frank. W. M., and E. A. Ritchie, 2001: Effects of vertical wind shear on the intensity and structure of numerically simulated hurricanes. *Mon. Wea. Rev.*, **129**, 2249-2269.

Gray, W. M., 1968: Global view of the origins of tropical cyclones. *Mon. Wea., Rev.*, **96**, 669-700.

Gray, W. M., 1975: Tropical cyclone genesis. Dept. of Atmos. Sci. Paper No. 234, Colo. State. Univ., Fort Collins, CO, 121 pp.

Haarsma, R. J., J. F. B. Mitchell, and C. A. Senior, 1993: Tropical disturbances in a GCM. *Climate Dynamics*, **8**, 247-257.

Hack, J. J., and W. H. Schubert, 1986: Nonlinear response of atmospheric vortices to heating by organized cumulus convection. *J. Atmos. Sci.*, **43**, 1559-1573.

Hendricks, E. A., M. T. Montgomery, and C. A. Davis, 2004: The role of "vortical" hot towers in the formation of Tropical Cyclone Diana (1984). *J. Atmos. Sci.*, **61**, 1209-1232.

Hong, S.-Y., J. Dudhia, and S.-H. Chen, 2004: A revised approach to ice microphysical processes for the parameterization of clouds and precipitation. *Mon. Wea. Rev.*, **132**, 103-120.

Hong, S.-Y., and J.-O. J. Lim, 2006: The WRF single-moment 6-class microphysics scheme (WSM6). *J. Korean Meteorol. Soc.*, **42**, 129-151.

Hong, S.-Y., and H.-L. Pan, 1996: Nonlocal boundary layer vertical diffusion in a medium-range forecast model. *Mon. Wea. Rev.*, **124**, 2322-2339.

Iacono, M. J., E. L. Mlawer, S. A. Clough, and J. J. Morcrette, 2000: Impact of an improved longwave radiation model, RRTM, on the energy budget and thermodynamics properties of the NCAR communicty climate model, CCM3. *J. Geophys. Res.*, **105 (D11)**, 14873-14890.

Kaplan, J. and M. DeMaria, 2003: Large-scale characteristics of rapidly intensifying tropical cyclones in the North Atlantic basin. *Wea. Forecasting*, **18**, 1093-1108.

Knutson, T. R., and R. E. Tuleya, 2004: Impact of CO2-induced warming on simulated hurricane intensity and precipitation: Sensitivity to the choice of climate model and convective parameterization. *J. Climate*, **17**, 3477-3495.

Knutson, T. R., R. E. Tuleya, W. Shen, and I. Ginis, 2001: Impact of CO2-induced warming on hurricane intensities as simulated in a hurricane model with ocean coupling. *J. Climate*, **14**, 2458-2468.

Laprise, R., 1992: The Euler equations of motion with hydrostatic pressure as an independent variable. *Mon. Wea. Rev.*, **120**,197-207.

Lighthill, J. G. Holland, W. Gray, C. Landsea, G. Craig, J. Evans, Y. Kurihara, and C. Guard, 1994: Global climate change and tropical cyclones. *Bull. Amer. Met. Soc.*, **75**, 2147-2157.

Liu, Y., D.-L. Zhang, and M. K. Yau, 1997: A multiscale numerical study of Hurricane Andrew (1992). Part I: Explicit simulation and verification. *Mon. Wea. Rev.*, **125**, 3073-3093.

Manabe, S., and R. F. Strickler, 1964: Thermal equilibrium of the atmosphere with a convective adjustment. *J. Atmos. Sci.*, **21**, 361-385.

McBride, J. L., 1981: Observational analysis of tropical cyclone formation. Part I: Basic definition of data sets. *J. Atmos. Sci.*, **38**, 1117-1131.

McBride, J. L., , and R. Zehr, 1981: Observational analysis of tropical cyclone formation. Part II: Comparison of non-developing versus developing systems. *J. Atmos. Sci.*, **38**, 1117-1131.

McDonald, R. E., D. G. Bleaken, D. R. Cresswell, V. D. Pope, and C. A. Senior, 2005: Tropical storms: representation and diagnosis in climate models and impacts of climate change. *Climate Dynamics*, **25**, 19-36.

Mlawer, E. J., S. J. Taubman, P. D. Brown, M. J. Iacono, and S. A. Clough, 1997: Radiative transfer for inhomogeneous atmosphere: RRTM, a validated correlated-k model for the longwave. *J. Geophys. Res.*, **102**(D14), 16663-16682.

Montgomery, M. T., M. E. Nicholls, T. A. Cram, and A. B. Saunders, 2006: A vortical hot tower route to tropical cyclogenesis. *J. Atmos. Sci.*, **63**, 355-386.

Noh, Y., W.-G. Cheon, S.-Y. Hong, and S. Raasch, 2003: Improvement of the K-profile model for the planetary boundary layer based on large eddy simulation data. *Bound.-Layer Meteor.*, **107**, 401-427.

Nolan, D. S., 2007: What is the trigger for tropical cyclogenesis? *Aust. Meteorol. Mag.,* accepted.

Nolan, D. S., Y. Moon, and D. P. Stern, 2007: Tropical cyclone intensification from asymmetric convection: Energetics and efficiency. *J. Atmos. Sci.*, in press.

Nolan, D. S., M. T. Montgomery, and L. D. Grasso, 2001: The wavenumber-one instability and trochoidal motion of huricane-like vortices. *J. Atmos. Sci.*, **58**, 3243-3270.

Nolan, D. S., Eric D. Rappin, and Kerry A. Emanuel, 2006: Could hurricanes form from random convection in a warmer world? *Preprints, 27th Conference on Hurricanes and Tropical Meteorology,* Monterey, CA, American Meteorological Society, Boston.

Oouchi, K. J. Yoshimura, H. Yoshimura, R. Mizuta, S. Kusunoki and A. Noda, 2006: Tropical cyclone climatology in a global-warming climate as simulated in a 20-km mesh global atmospheric model: Frequency and wind intensity analysis. *J. Meteorol. Soc. Japan*, **84**, 259-276.

Ooyama, K., 1969: Numerical simulation of the life cycle of tropical cyclones. *J. Atmos. Sci.*, **26**, 3-40.

Ooyama, K., 1982: A dynamical model for the study of tropical cyclone development. *Geofys. Int.*, **4**, 187-198.

Palmen, E. H., 1948: On the formation and structure of tropical cyclones. *Geophysica*, **3**, 26-28.

Pauluis, O., and S. Garner, 2006: Sensitivity of radiative-convective equilibrium simulations to horizontal resolution. *J. Atmos. Sci.*, **63**, 1910-1923.

Persing, J., and M. T. Montgomery, 2003: Hurricane superintensity. *J. Atmos. Sci.*, **60**, 2349-2371.

Reasor, P. D., M. T. Montgomery, and L. F. Bosart, 2005: Mesoscale observations of the genesis of Hurricane Dolly (1996). *J. Atmos. Sci.*, **62**, 3151-3171.

Robe, F. R., and K. A. Emanuel, 2001: The effect of vertical wind shear on radiative-convective equilibrium states. *J. Atmos. Sci.*, **58**, 1427-1445.

Romine, G. S., and R. B. Wilhelmson, 2006: Finescale spiral band features within a numerical simulation of Hurricane Opal (1995). *Mon. Wea. Rev.*, **134**, 1121-1139.

Rogers, R., S. Chen, J. Tenerelli, and H. Willoughby, 2003: A numerical study of the impact of vertical shear on the distribution of rainfall in Hurricane Bonnie (1998). *Mon. Wea. Rev.*, **131**, 1577-1599.

Rotunno, R., and K. A. Emanuel, 1987: An air-sea interaction theory for tropical cyclones. Part II: Evolutionary study using a nonhydrostatic axisymmetric mumerical model. *J. Atmos. Sci.*, **44**, 542-561.

Royer, J.-F., F. Chauvin, B. Timbal, P. Araspin, and D. Grimal, 1998: *Climatic Change*, **38**, 307-343.

Ryan, B. F., I. G. Watterson, and J. L. Evans, 1992: Tropical cyclone frequencies inferred from Gray's yearly genesis parameter: Validation of GCM tropical climates. *Geophsy. Res. Lett.*, **19**, 1831-1834.

Shen, W., R. E. Tulyea, and I. Ginis, 2000: A sensitivity study of the thermodynamic environment on GFDL model hurricane intensity: Implications for global warming. *J. Climate*, **13**, 109-121.

Simpson, J., E. Ritchie, G. J. Holland, J. Halverson, and S. Stewart, 1997: Mesoscale interatcions in tropical cyclone genesis. *Mon. Wea. Rev.*, **125**, 2643-2661.

Simpson, R. H., and H. Riehl, 1958: Midtropospheric ventilation as a constraint on hurricane development and maintenance. *Proceedings of the AMS Technical Conference on Hurricanes*, Miami, Florida, D41-D410.

Sippel, J. A., J. W. Nielsen-Gammon, and S. E. Allen, 2006: The multiple-vortex nature of tropical cyclogenesis. *Mon. Wea. Rev.*, **134**, 1796-1814.

Skamarock, W. C., J. B. Klemp, J. Dudhia, D. O. Gill, D. M. Barker, W. Wang, and J. G. Powers, 2005: *A Description of the Advanced Research WRF Version 2*. NCAR technical note 468+STR, 88 pp.

Sugi, M., A. Noda, and N. Sato, 2002: Influence of the global warmine on tropical cyclone climatology: An experiment with the JMA model. *J. Meteorol. Soc. Japan*, **80**, 249-272.

Tompkins, A. M., and G. C. Craig, 1998a: Radiative-convective equilibrium in a three-dimensional cloud-ensemble model. *Q. J. R. Meteorol. Soc.*, **124**, 2073-2097.

Tompkins, A. M., and G. C. Craig, 1998b: Time-scales of adjustment to radiative-convective equilibrium in the tropical atmosphere. *Q. J. R. Meteorol. Soc.*, **124**, 2073-2097.

Tompkins, A. M., 2001: Organization of tropical convection in low wind shears: The role of water vapor. *J. Atmos. Sci.*, **58**, 529-545.

Vecchi, G. A., and B. J. Soden, 2007: Increased tropical Atlantic wind shear in model projections of global warming. *Geophys Res. Lett.*, **34**, L08702, doi:10.1029/2006GL028905.

Watterson, I. G., J. L. Evans, and B. F. Ryan, 1995: Seasonal and interannual variability of tropical cyclogenesis: Diagnostics from large-scale fields. *J. Climate*, **8**, 3052-3066.

Wallace, J. M., and P. V. Hobbs, 2006: *Atmospheric Science: An Introductory Survey.* Academic Press, New York, 483 pp.

Wang, Y., 2002: Vortex Rossby waves in a numerically simulated tropical cyclone. Part I: Overall structure, potential vorticity, and kinetic energy budgets. *J. Atmos. Sci.*, **59**, 1213-1238.

Wicker, L. J., and W. C. Skamarock, 2002: Time-splitting methods for elastic models using forward time schemes. *Mon. Wea. Rev.*, **130**, 2088-2097.

Yano, J.-I., and K. A. Emanuel, 1991: An improved model of the equatorial troposphere and its coupling with the stratosphere. *J. Atmos. Sci.*, **48**, 377-389.

Yoshimura, J. S. Masato, and A. Noda, 2006: Influence of greenhouse warming on tropical cyclone frequency. *J. Meteorol. Soc. Japan*, **84**, 405-428.

Table 1 Values of CAPE (Jkg^{-1}), V_{pot} (m/s), and genesis index for RCE with u_m = 3.0 m/s.

	SST = 25.0 C	27.5 C	30.0 C
$f = 0.25x10^{-4}s^{-1}$	1167 64.5 11	1522 68.8 13	2020 72.3 16
$0.5x10^{-4}s^{-1}$	1078 63.8 24	1523 66.9 35	1992 70.6 42
$0.75x10^{-4}s^{-1}$	1117 63.3 45	1552 66.7 66	2011 70.2 74

Table 1: Thermodynamic and genesis parameters for atmospheres generated by small-domain simulations of RCE with various values of the environmental parameters SST and f, with u_m = 3.0 ms^{-1}. Beginning from the top in each cell, the numbers are CAPE in Jkg^{-1}, V_{pot} in ms^{-1}, and the genesis index *GP*.

Table 2 Values of CAPE (J/kg), V_{pot} (m/s), and genesis index for RCE with $f = 0.5 \times 10^{-4}$ s^{-1}.

	SST = 25 C	27.5 C	30.0 C
u_m = 1.0 m/s	268 77.2 16	446 83.3 22	550 87.7 31
2.0	713 70.6 24	959 75.5 33	1193 79.4 40
3.0	1078 63.8 24	1523 66.9 35	1992 70.6 42
4.0	1471 57.4 22	1886 60.7 26	2467 64.4 36
5.0	1738 52.8 18	2285 55.6 23	2933 58.9 30

Table 2: As in Table 1, but for $f = 5.0 \times 10^{-5}$ s^{-1}, and for various values of SST and u_m. Beginning from the top in each cell, the numbers are CAPE in J kg^{-1}, V_{pot} in ms^{-1}, and *GP*.

Table 3 Objective genesis and rapid intensification times for the initial-vortex simulations.

Simulation	SST (C)	f ($\times 10^{-4}$ s^{-1})	u_m (ms^{-1})	time to genesis (h)	time to most rapid intensification (h)
Control	27.5	0.5	3.0	42	88
SST 25	25.0			54	117
SST 30	30.0			39	68
low f		0.25		54	100
high f		0.75		68	104
low u_m			1.0	36	78
high u_m			5.0	70	125

Figure Captions

Figure 1: Illustration of the states of radiative-convective-equilibrium in the small-domain simulations: a) Time evolution of domain-averaged moist state energy (MSE); with snapshots in equilibrium for b) vertical velocity; c) θ_e on the lowest model level; and d) water vapor path.

Figure 2: Vertical profiles of (a) temperature and (b) relative humidity for small-domain, RCE simulations for SST = 25, 27.5, and 30 C.

Figure 3: Vertical profiles of (a) temperature and (b) relative humidity for small-domain, RCE simulations for mean surface wind u_m = 1, 3, and 5 ms^{-1}.

Figure 4: Radius-height cross-section of the azimuthal wind field for the initial vortices used in this study. Units are ms^{-1}.

Figure 5: Results from initial-vortex simultions for varying values of the SST: a) maximum surface wind speed; b) minimum surface pressure. The three lines for SST = 27.5 C marked (a), (b), and (c) in each figure are for three simulations with different random noise in their initial temperature fields.

Figure 6: Hovmoller diagrams of the azimuthally averaged 10 m wind for three initial-vortex simulations with varying SST. Wind speeds have been normalized by V_{pot} for each case, and the contour interval for the normalized velocity is 0.078.

Figure 7: Hovmoller diagrams for the initial vortex simulations with varying SST: a) azimuthally averaged vertical vorticity at z = 2.2 km; d) azimuthally averaged vertical velocity at z = 5 km. Vertical winds have been normalized by V_{pot} for each case (contour interval 0.0056) , while vorticity has been normalized by f (contour interval 12.8).

Figure 8: Results from initial-vortex simulations for varying values of the Coriolis parameter f: a) maximum surface wind speed; b) minimum surface pressure; c) Hovmoller diagram of the azimuthally averaged vertical vorticity at z = 2.2 km; d) Hovmoller diagram of the azimuthally averaged vertical velocity at z = 5 km. Vertical winds have been normalized by V_{pot} for each case, while vorticity has been normalized by f, with the same contour intervals as above.

Figure 9: Results from initial-vortex simultions for varying values of the mean surface wind um: a) maximum surface wind speed; b) minimum surface pressure; c) Hovmoller diagram of the azimuthally averaged vertical vorticity at z = 2.2 km; d) Hovmoller diagram of the azimuthally averaged vertical velocity at z = 5 km. Vertical winds have been normalized by V_{pot} for each case, while vorticity has been normalized by f, with the same contour intervals as above.

Figure 10: Minimum surface pressure (upper panel) and maximum 10 m wind speed (lower panel) for the control simulation, and for two simulations with weaker initial vortices, with v_{max} = 2.5 ms^{-1} and v_{max} = 1.25 ms^{-1}.

Figure 11: Minumum surface pressure (upper panel) and maximum 10 m wind speed (lower panel) for the spontaneous genesis simulation.

Figure 12: Water vapor path (WVP) at $t = 4$, 6, 8, and 10 days for the spontaneous genesis simulation.

Figure 13: Vertical vorticity at $z = 2.2$ km for $t = 11$, 12, 13, and 14 days of the spontaneous genesis case.

Figure 14: Results of a quartile analysis, as in Bretherton et al. (2005), based on water vapor path (WVP) over 400 equal size sub-grids of the model domain in the spontaneous genesis simulation. Dotted curves are data from subgrids with the first quartile of WVP values, dash-dot are the second quartile, dashed the third, thin-solid the fourth, and thick-solid lines are means over the entire domain: a) WVP; b) outgoing longwave radiation; c) vertical velocity at $z = 5$ km; d) vertical vorticity at $z = 2$ km; e) water vapor flux in terms of latent heat energy; f) precipitation.

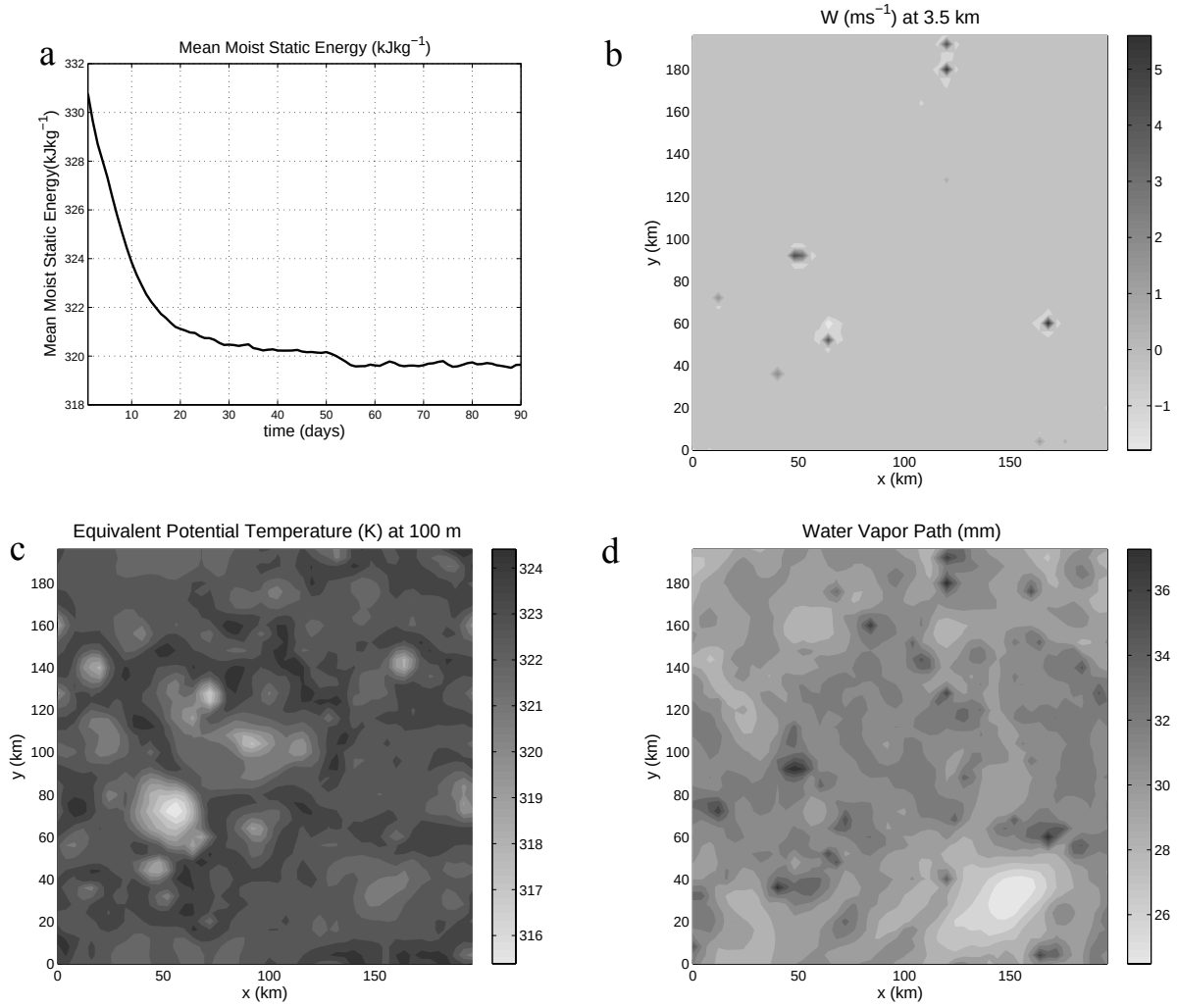

Fig. 1 Illustration of the states of radiative-convective-equilibrium in the small-domain simulations: a) Time evolution of domain-averaged moist state energy (MSE); with snapshots in equilibrium for b) vertical velocity; c) θ_e on the lowest model level; and d) water vapor path.

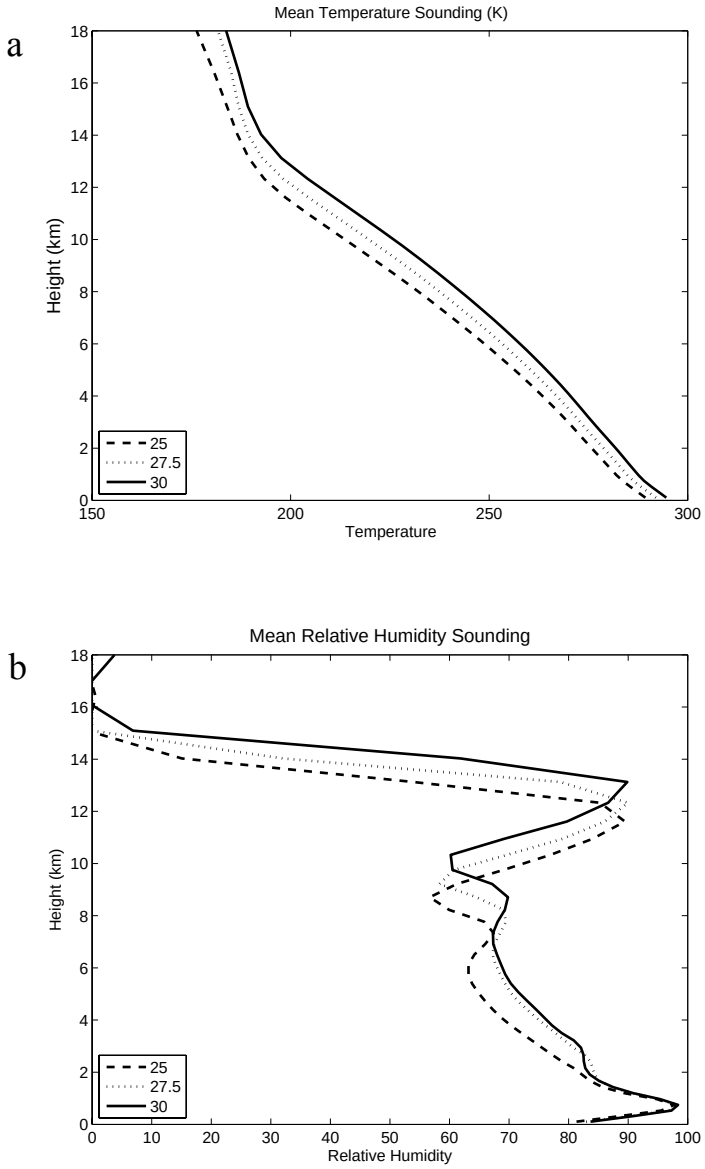

Fig. 2 Vertical profiles of (a) temperature and (b) relative humidity for small-domain, RCE simulations for SST = 25, 27.5, and 30 C.

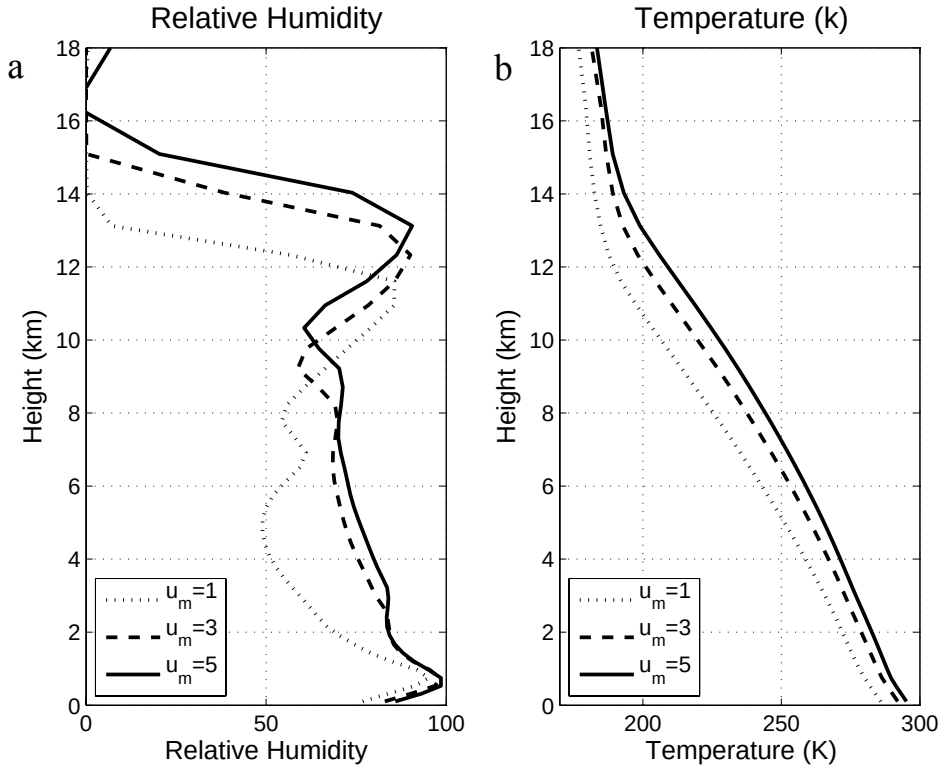

Fig. 3 Vertical profiles of (a) temperature and (b) relative humidity for small-domain, RCE simulations for mean surface wind u_m = 1, 3, and 5 ms^{-1}.

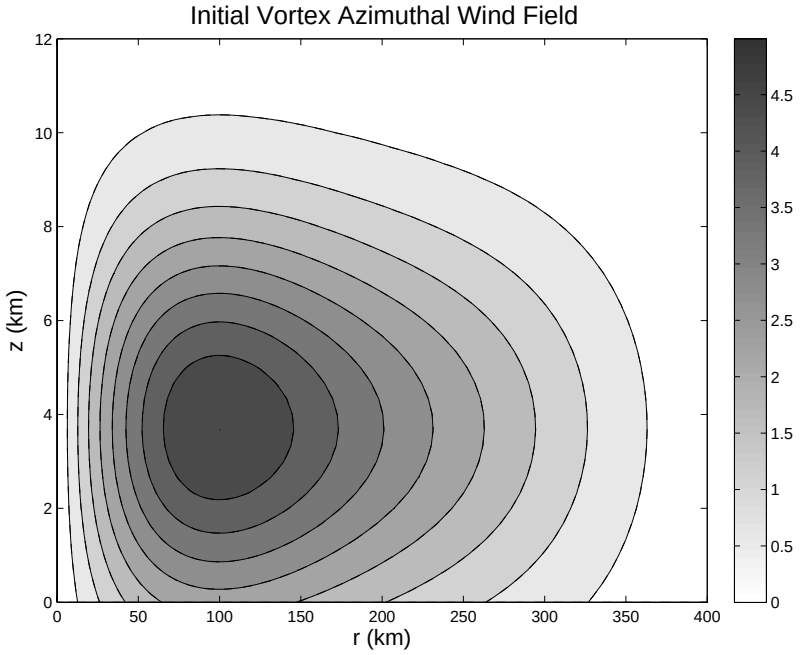

Fig. 4 Radius-height cross-section of the azimuthal wind field for the initial vortices used in this study. Units are ms^{-1}.

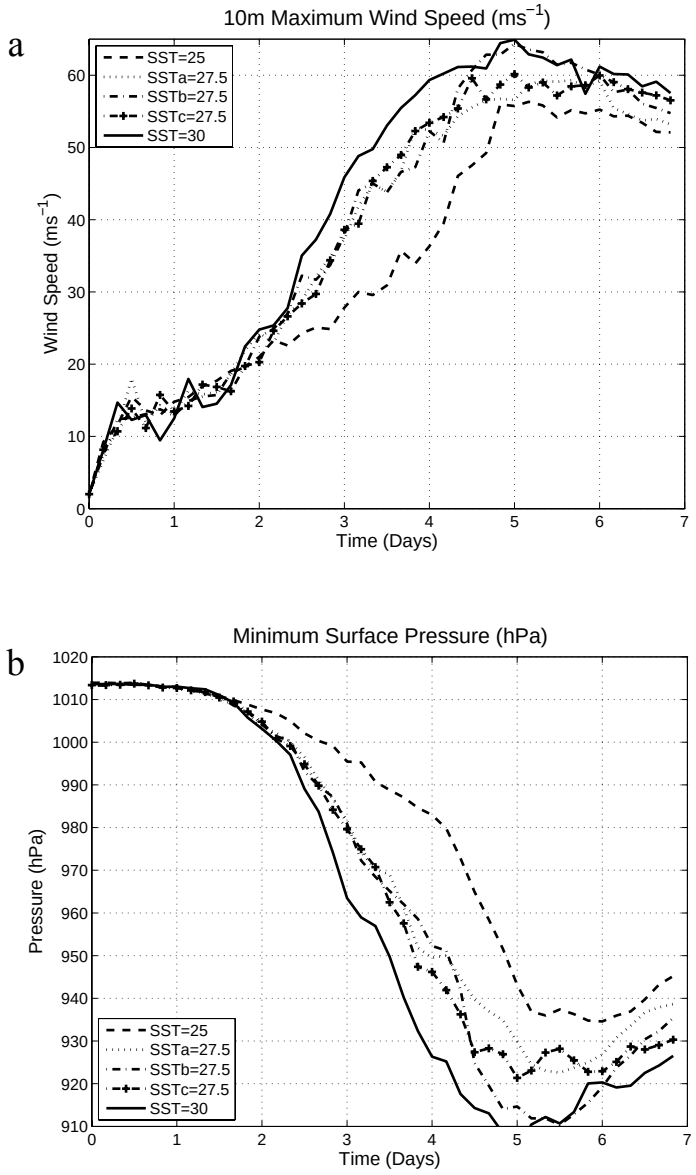

Fig. 5 Results from initial-vortex simultions for varying values of the SST: a) maximum surface wind speed; b) minimum surface pressure. The three lines for SST = 27.5 C marked (a), (b), and (c) in each figure are for three simulations with different random noise in their initial temperature fields.

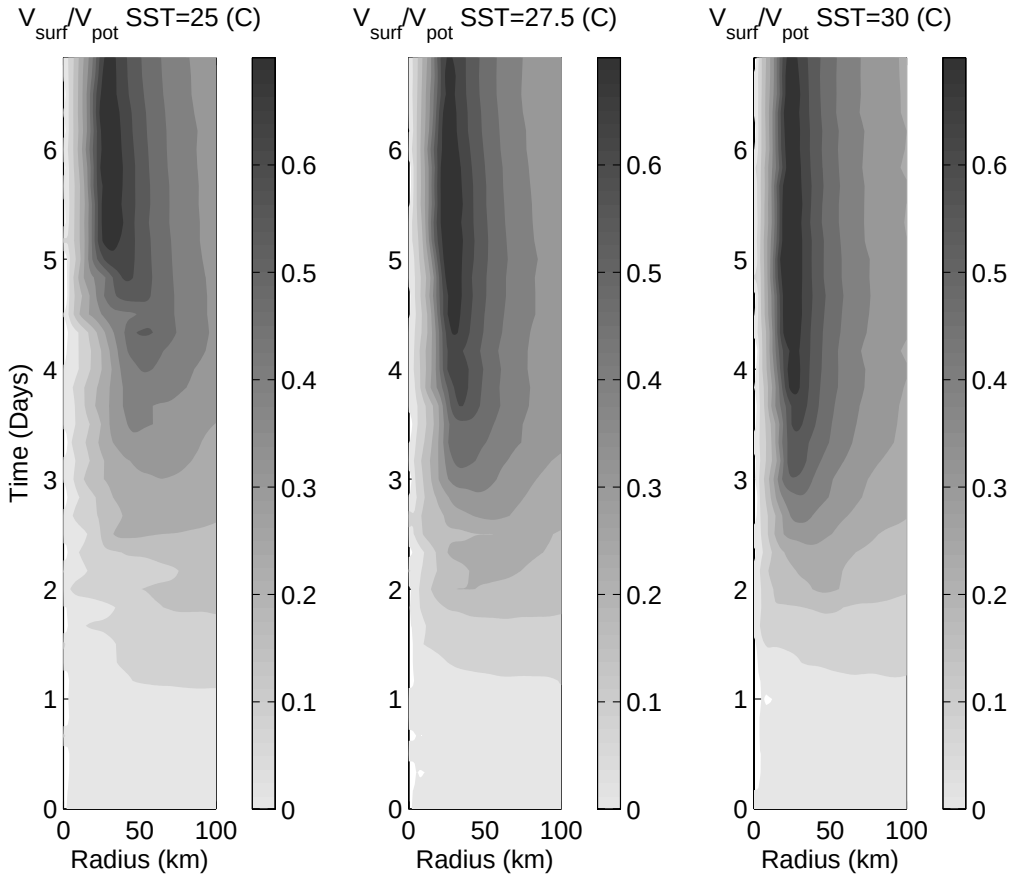

Fig. 6 Hovmoller diagrams of the azimuthally averaged 10 m wind for three initial-vortex simulations with varying SST. Wind speeds have been normalized by V_{pot} for each case, and the contour interval for the normalized velocity is 0.078.

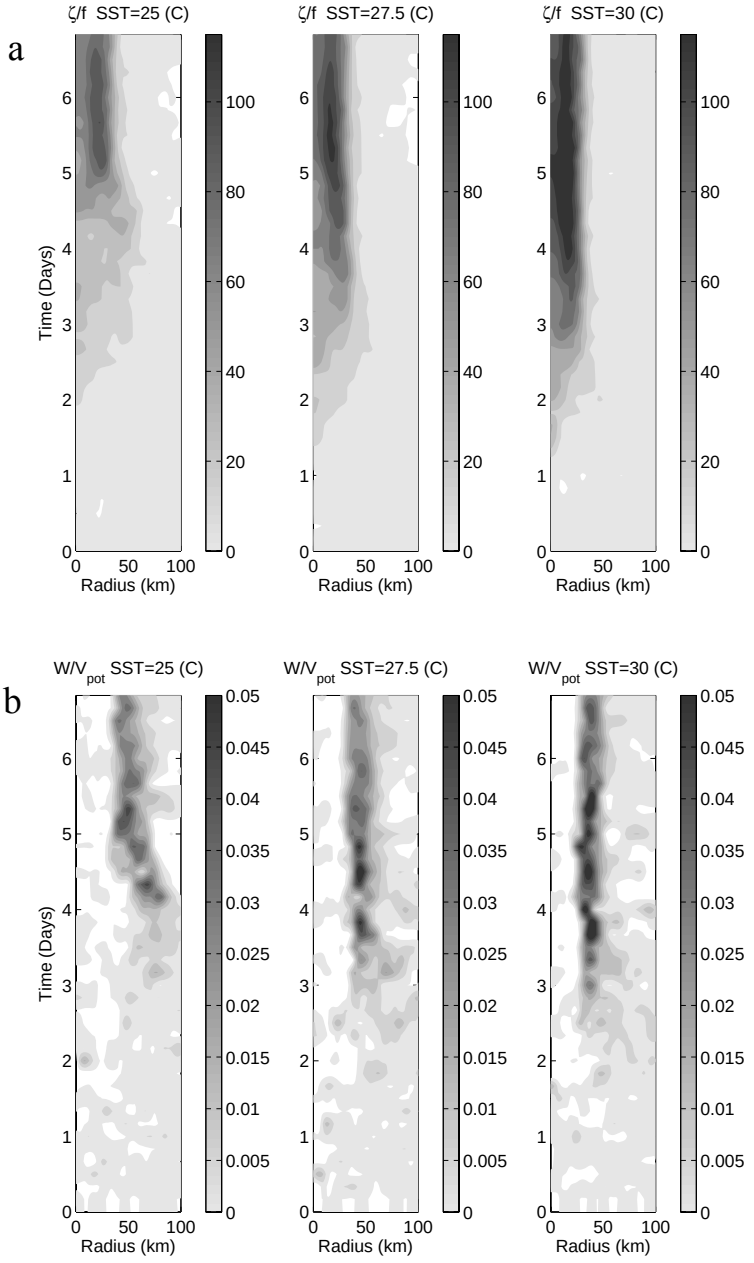

Fig. 7 Hovmoller diagrams for the initial vortex simulations with varying SST: a) azimuthally averaged vertical vorticity at $z = 2.2$ km; d) azimuthally averaged vertical velocity at $z = 5$ km. Vertical winds have been normalized by V_{pot} for each case (contour interval 0.0056) , while vorticity has been normalized by f (contour interval 12.8).

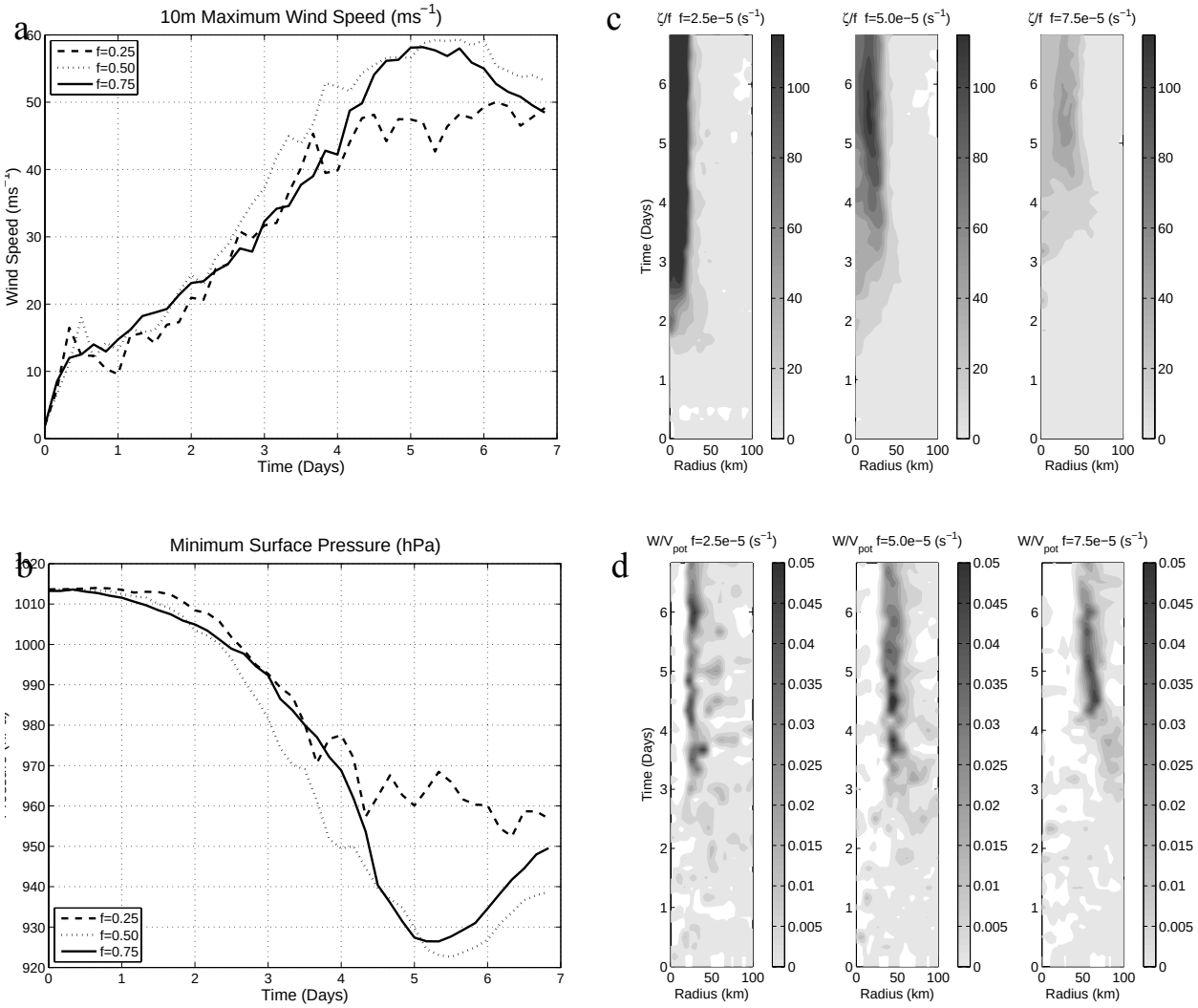

Fig. 8 Results from initial-vortex simulations for varying values of the Coriolis parameter *f*: a) maximum surface wind speed; b) minimum surface pressure; c) Hovmoller diagram of the azimuthally averaged vertical vorticity at $z = 2.2$ km; d) Hovmoller diagram of the azimuthally averaged vertical velocity at $z = 5$ km. Vertical winds have been normalized by V_{pot} for each case, while vorticity has been normalized by *f*, with the same contour intervals as above.

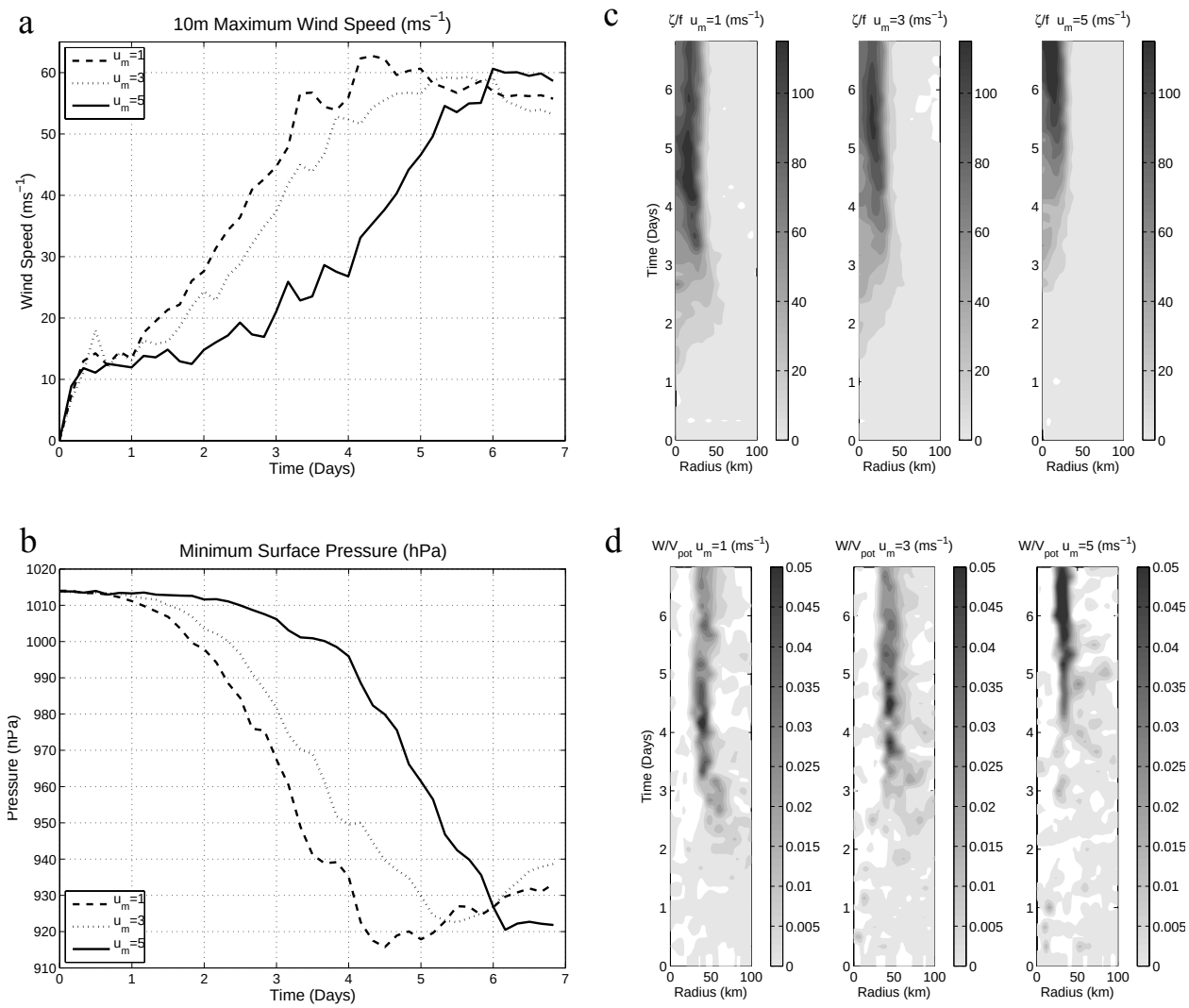

Fig. 9 Results from initial-vortex simultions for varying values of the mean surface wind um: a) maximum surface wind speed; b) minimum surface pressure; c) Hovmoller diagram of the azimuthally averaged vertical vorticity at z = 2.2 km; d) Hovmoller diagram of the azimuthally averaged vertical velocity at z = 5 km. Vertical winds have been normalized by V_{pot} for each case, while vorticity has been normalized by f, with the same contour intervals as above.

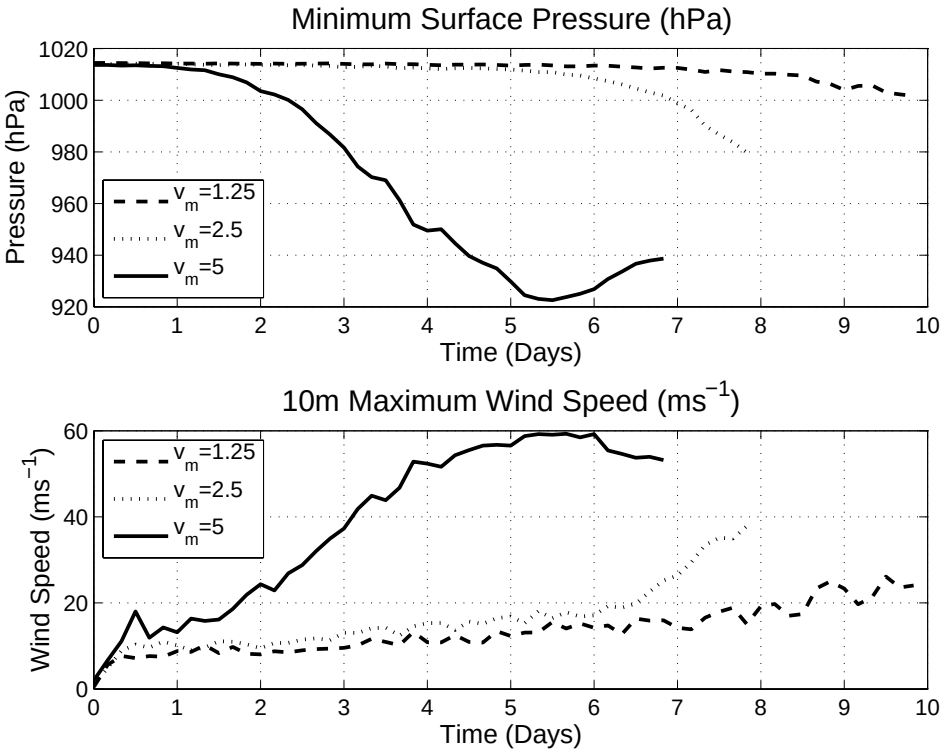

Fig. 10 Minimum surface pressure (upper panel) and maximum 10 m wind speed (lower panel) for the control simulation, and for two simulations with weaker initial vortices, with $v_{\max} = 2.5$ ms^{-1} and $v_{\max} = 1.25$ ms^{-1}.

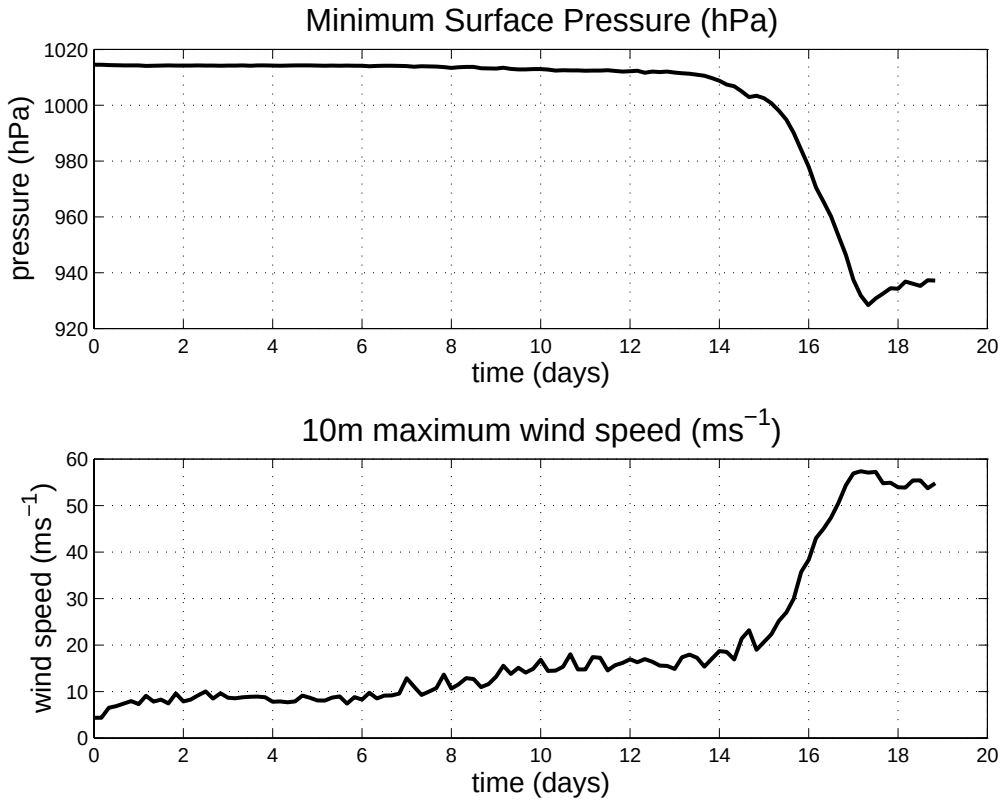

Fig. 11 Minumum surface pressure (upper panel) and maximum 10 m wind speed (lower panel) for the spontaneous genesis simulation.

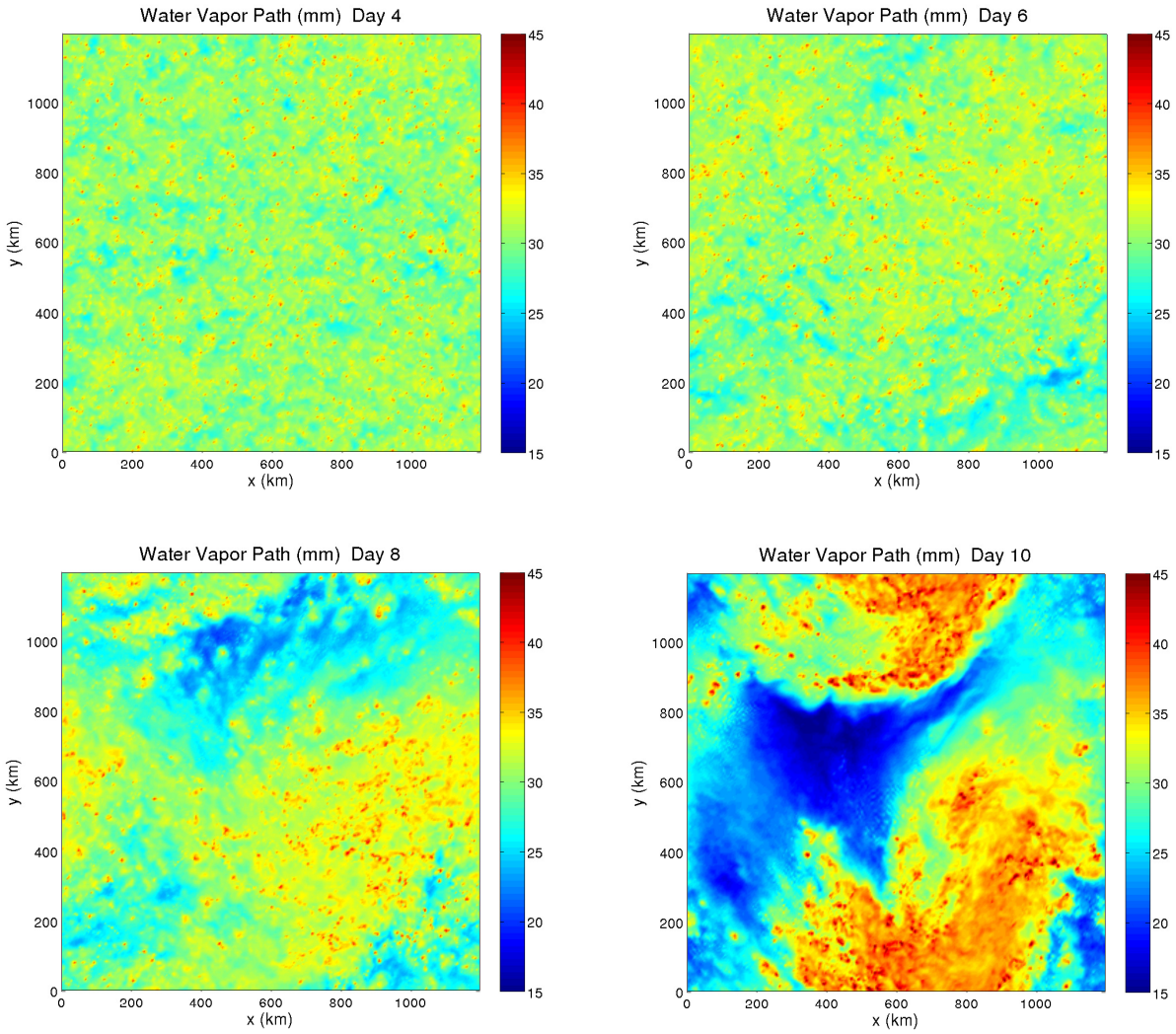

Fig. 12 Water vapor path (WVP) at $t = 4$, 6, 8, and 10 days for the spontaneous genesis simulation.

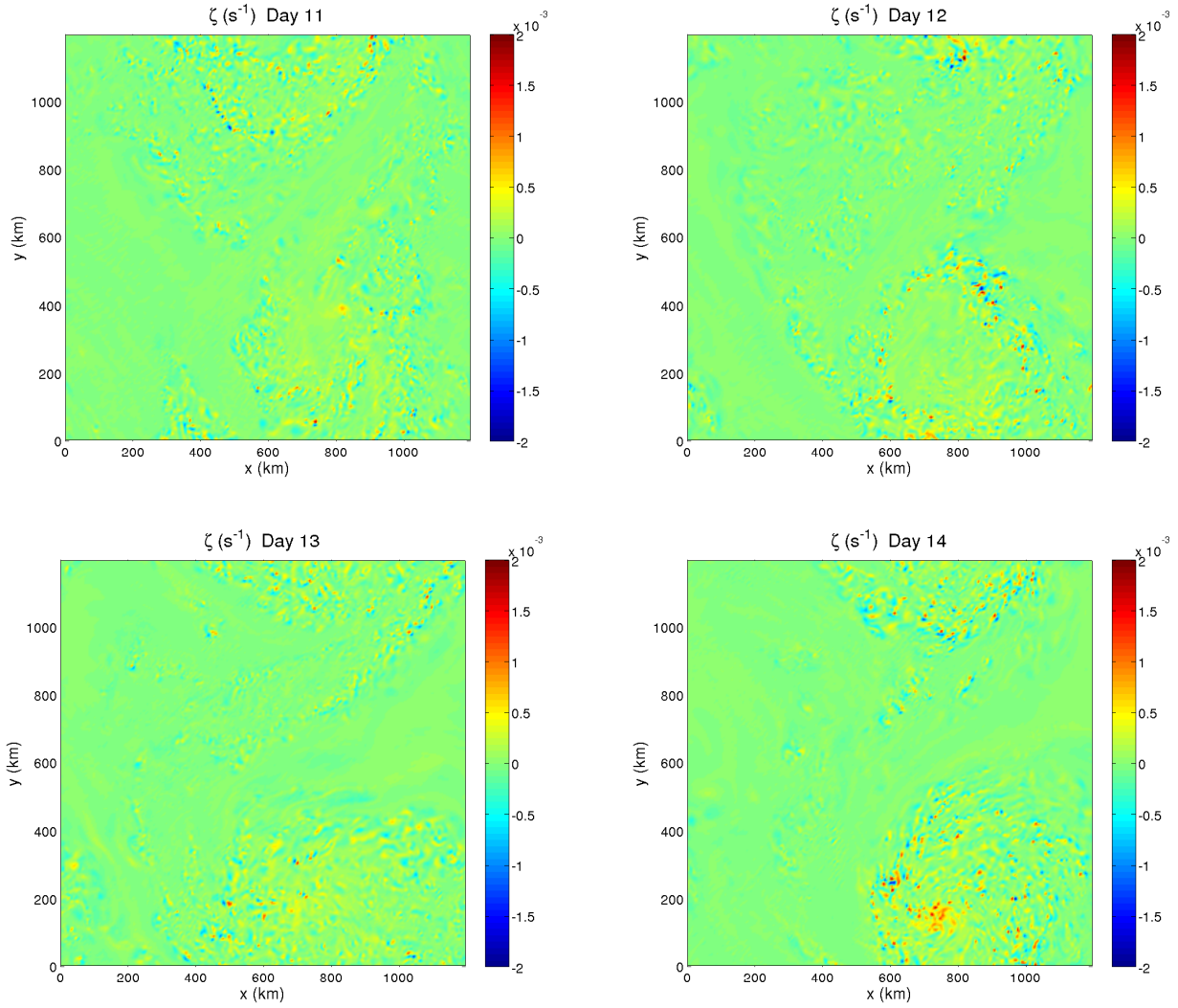

Fig. 13 Vertical vorticity at z = 2.2 km for t = 11, 12, 13, and 14 days of the spontaneous genesis case.

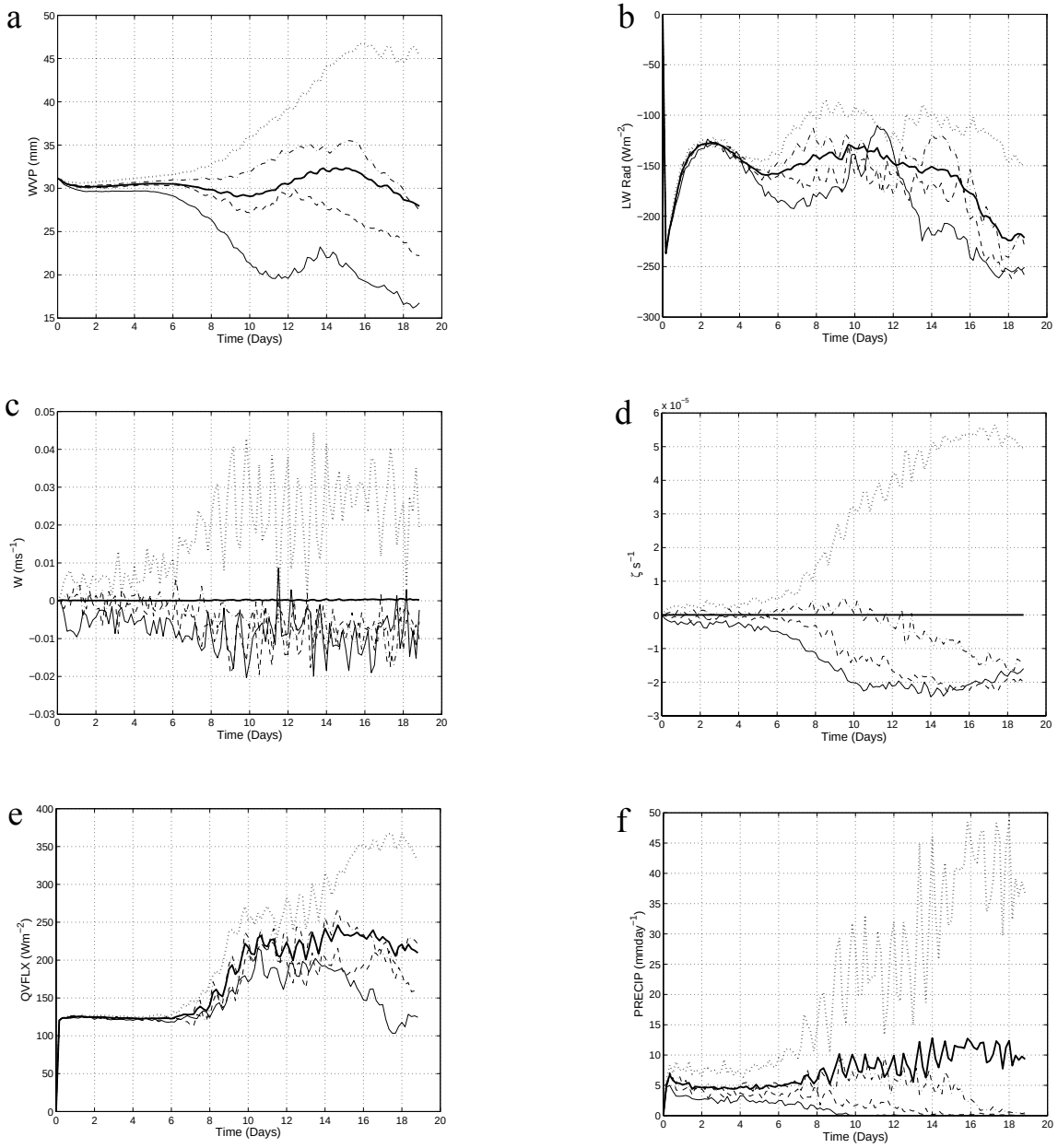

Fig. 14 Results of a quartile analysis, as in Bretherton et al. (2005), based on water vapor path (WVP) over 400 equal size sub-grids of the model domain in the spontaneous genesis simulation. Dotted curves are data from subgrids with the first quartile of WVP values, dash-dot are the second quartile, dashed the third, thin-solid the fourth, and thick-solid lines are means over the entire domain: a) WVP; b) outgoing longwave radiation; c) vertical velocity at z = 5 km; d) vertical vorticity at z = 2 km; e) water vapor flux in terms of latent heat energy; f) precipitation.